Atmos. Meas. Tech., 5, 1491–1511, 2012
www.atmos-meas-tech.net/5/1491/2012/
doi:10.5194/amt-5-1491-2012

Atmospheric Measurement Techniques

Measuring variations of $\delta^{18}O$ and $\delta^{2}H$ in atmospheric water vapour using two commercial laser-based spectrometers: an instrument characterisation study

F. Aemisegger[1], P. Sturm[2,3], P. Graf[1], H. Sodemann[1], S. Pfahl[1], A. Knohl[2,4], and H. Wernli[1]

[1]Institute for Atmospheric and Climate Sciences, ETH Zurich, Switzerland
[2]Institute of Agricultural Sciences, ETH Zurich, Switzerland
[3]Empa, Swiss Federal Laboratories for Materials Science and Technology,
Laboratory for Air Pollution and Environmental Technology, Dübendorf, Switzerland
[4]Faculty of Forest Sciences and Forest Ecology – Bioclimatology, Georg-August University of Göttingen, Germany

Correspondence to: F. Aemisegger (franziska.aemisegger@env.ethz.ch)

Received: 25 January 2012 – Published in Atmos. Meas. Tech. Discuss.: 15 February 2012
Revised: 31 May 2012 – Accepted: 6 June 2012 – Published: 2 July 2012

Abstract. Variations of stable water isotopes in water vapour have become measurable at a measurement frequency of about 1 Hz in recent years using novel laser spectroscopic techniques. This enables us to perform continuous measurements for process-based investigations of the atmospheric water cycle at the time scales relevant for synoptic and mesoscale meteorology. An important prerequisite for the interpretation of data from automated field measurements lasting for several weeks or months is a detailed knowledge about instrument properties and the sources of measurement uncertainty. We present here a comprehensive characterisation and comparison study of two commercial laser spectroscopic systems based on cavity ring-down spectroscopy (Picarro) and off-axis integrated cavity output spectroscopy (Los Gatos Research). The uncertainty components of the measurements were first assessed in laboratory experiments, focussing on the effects of (i) water vapour mixing ratio, (ii) measurement stability, (iii) uncertainties due to calibration and (iv) response times of the isotope measurements due to adsorption-desorption processes on the tubing and measurement cavity walls. Based on the experience from our laboratory experiments, we set up a one-week field campaign for comparing measurements of the ambient isotope signals from the two laser spectroscopic systems. The optimal calibration strategy determined for both instruments was applied as well as the correction functions for water vapour mixing ratio effects. The root mean square difference between the isotope signals from the two instruments during the field deployment was 2.3 ‰ for $\delta^{2}H$, 0.5 ‰ for $\delta^{18}O$ and 3.1 ‰ for deuterium excess. These uncertainty estimates from field measurements compare well to those found in the laboratory experiments. The present quality of measurements from laser spectroscopic instruments combined with a calibration system opens new possibilities for investigating the atmospheric water cycle and the land-atmosphere moisture fluxes.

1 Introduction

The atmospheric transport patterns of water vapour significantly influence local climates and Earth's surface hydrology. As naturally available tracers of phase transitions of water, stable isotopes provide useful information on the atmospheric water cycle, in particular on conditions during phase changes such as evaporation from the sea surface (Pfahl and Wernli, 2008; Sodemann et al., 2008; Uemura et al., 2008), plant transpiration (Farquhar et al., 2007), cloud formation (Federer et al., 1982; Ciais and Jouzel, 1994) and post-condensation exchange with below cloud vapour (Field et al., 2010). To investigate these processes and their impact on stable water isotopes in atmospheric waters at the temporal scale of significant weather events, high frequency measurements of stable water isotopes are essential. Such measurements can also help to validate model

parametrisations of evaporation (He and Smith, 1999), transpiration (Dongmann et al., 1974) and rainfall re-evaporation (Lee and Fung, 2008).

Stable water isotope measurements in liquid waters have been used for several decades as a means to probe the hydrologic cycle and to gain insight into its fundamental processes (Gat, 1996). The International Atomic Energy Agency (IAEA) and the World Meteorological Organisation (WMO) have been surveying the content of hydrogen and oxygen isotopes in precipitation since 1961 in the framework of their Global Network on Isotopes in Precipitation (GNIP; Araguas et al., 1996). The key mechanisms influencing the abundance of heavy water isotopes in meteoric waters on relatively long, typically monthly timescale have subsequently been identified (Craig, 1961; Dansgaard, 1964; Gat and Dansgaard, 1972). The dependency of the isotopic composition of precipitation on meteorological conditions during phase changes has been used for inferring information about past climate from paleo-archives (Dansgaard et al., 1993; Jouzel et al., 1997; Johnsen et al., 2001).

Stable isotopes have been less extensively measured in water vapour than in the liquid phase, mainly because such measurements have been very laborious and error-prone until recently (Helliker and Noone, 2010), involving cryogenic trapping with vacuum flasks (e.g. Yakir and Wang, 1996; Gat et al., 2003; Yepez et al., 2003; Strong et al., 2007) or collection with molecular sieves (Han et al., 2006) followed by isotope ratio mass spectrometric (IRMS) analysis. Besides the extensive effort for sample preparation, involving chemical conversion or isotopic equilibration with a gas-like CO_2, these measurements are limited in throughput (Horita and Kendall, 2004). With recent progress in optical laser systems, point measurements of stable water isotopes in water vapour with a high temporal resolution in the order of seconds have become possible, overcoming many disadvantages of traditional mass spectrometric measurements. The availability of relatively compact field-deployable laser spectroscopic instruments, simultaneously measuring $^1H_2{}^{16}O$, $^2H^1H^{16}O$ and $^1H_2{}^{18}O$ isotopes, allows performing online, autonomous and long-term point measurements of the stable water isotope composition of atmospheric vapour.

Several research instruments (Webster and Heymsfield, 2003; Kerstel et al., 2006; Sayres et al., 2009; Dyroff, 2010) and commercial measurement systems (Picarro, www.picarro.com; Los Gatos Research, www.lgrinc.com) based on cavity ring-down, cavity enhanced and tunable diode laser absorption spectroscopy have been proposed in the last decade. Kerstel and Gianfrani (2008) gave a thorough review of recent advances in infrared isotope ratio spectroscopy and the main applications of this technology. Spectral selectivity and the sensitivity of the optical components as well as electronic noise associated with the setup limit the precision of infrared isotope ratio measurements (Paldus and Kachanov, 2005). Many recent studies indicate similar performance of laser and conventional IRMS systems in terms of precision (Kerstel et al., 2006; Gupta et al., 2009; Sturm and Knohl, 2010). Equally relevant for atmospheric field applications, however, is the overall measurement uncertainty resulting from a range of factors like calibration, sensitivity to variations in water concentration, and retention effects from the tubing (Brand et al., 2009; Schmidt et al., 2010; Johnson et al., 2011; Rambo et al., 2011). Thus, a detailed assessment of the novel laser instruments and testing of their performance in field conditions is necessary to fully characterise the measurement uncertainty and to correct for biasing effects.

Here, we present results from a characterisation and intercomparison study of two commercial laser spectroscopic instruments for high frequency measurements of the three stable water isotopes $^1H_2{}^{16}O$, $^1H_2{}^{18}O$ and $^2H^1H^{16}O$ in water vapour. Our primary aim is to provide a complete uncertainty assessment for the Picarro L1115-i system. A second laser spectroscopic instrument, the WVIA by Los Gatos Research, which was extensively characterised by Sturm and Knohl (2010), is used for comparison in a slightly modified setup (improved temperature stabilisation and slightly different water vapour mixing ratio dependency). The two latest versions (L2130-i and WVIA-EP) of both systems were tested as well, and our findings concerning instrument improvements will be discussed. The proposed assessment considers four important aspects: (1) an inter-comparison of measurement quality between the two analysers and with IRMS is done using 10 liquid standards; (2) the water vapour mixing ratio dependencies of isotope measurements are quantified; (3) the stability of the systems in terms of precision as well as in terms of optimal calibration frequency is investigated; and (4) the response times of the measurement systems after a step change in isotope and water concentration are characterised. The structure of this paper follows the description and evaluation of these 4 characterisation steps. At the end a short case study is presented of comparative ambient air measurements in field conditions with the two laser systems operated in a way that was found optimal during the laboratory tests.

2 Instrumentation

2.1 Quantification of the isotopic content of water samples

The heavy isotopic content of a given water vapour sample is generally expressed in terms of relative deviation of the isotopic mixing ratio from an internationally accepted standard:

$$\delta = \frac{R_{\text{sample}} - R_{\text{standard}}}{R_{\text{standard}}}, \quad (1)$$

where R represents the ratio of the rare, heavy isotopic concentration ($^2H^1H^{16}O$ or $^1H_2{}^{18}O$) to the concentration of the

Table 1. Properties and technical details of the L1115-i, L2130-i (Picarro) and the WVIA (Los Gatos) laser systems. The WVIA-EP instrument has a smaller cavity than the WVIA, different ring-down times, laser path lengths but similar power consumption (200 W).

Properties	Picarro	Los Gatos
Technology	CRDS[1)]	OA-ICOS[2)]
Spectral domain	7183.5–7184 (in 0.01 cm^{-1} steps)	7199.9–7200.4 cm^{-1} (in 7×10^{-5} cm^{-1} steps)
Absorption path length	∼ 12 km	∼ 7 km
Ring down time	40 µs	24 µ s
Cavity size	35 ccm	∼830 ccm
Cavity pressure	46.66 ± 0.03 hPa	50 ± 0.007 hPa
Cavity temperature	80 ± 0.002°C	$\sim 47 \pm 0.002$°C
Pumping rate	25 ml min^{-1}	500–800 ml min^{-1}
Cavity exchange rate	8 s	2–3 s
Measurement frequency	0.5 Hz (1 Hz*)	2 Hz
H_2O range	6000 to 26 000 ppmv	4000 to 60 000 ppmv**
Volume	∼130 l	∼200 l
Power consumption	∼300 W with calibration 500 W	∼180 W (WVIA), 300 W (WVISS)

1 cavity ring-down spectroscopy. 2 off-axis integrated cavity output spectroscopy. * L2130-i. ** non-condensing

most abundant, lighter species ($^1H_2{}^{16}O$). The δ values are generally indicated in per mil. The internationally accepted primary standard defining the scale zero is known as the Vienna Standard Mean Ocean Water (VSMOW; Gonfiantini, 1978) distributed by the IAEA. $R_{standard}$ is the atomic isotopic ratio of VSMOW. When measuring isotopic composition of water samples, the delta values have to be normalised according to the IAEA VSMOW2-SLAP2 scale as described in IAEA (2009), which corresponds to a two point calibration with a fixed zero point (VSMOW) and a second reference point (SLAP, Standard Light Antarctic Precipitation).

2.2 Laser spectroscopic measurements of stable water isotopes in water vapour

Two physically different measurement principles allow to quantify the isotopic composition of natural waters. Isotope ratio mass spectrometry (IRMS) takes advantage of the differing mass-to-charge ratio of isotopes (Horita and Kendall, 2004). Laser spectroscopic systems use the difference in rotational-vibrational energy level structure of the different isotopic molecules, leading to isotope characteristic transition frequencies in the near-infrared region of the spectrum (Kerstel, 2004). Three nearby absorption peaks in the near-infrared region corresponding to the three molecules $^2H^1H^{16}O$, $^1H_2{}^{18}O$, and $^1H_2{}^{16}O$, are scanned by a laser in continuous wave operation mode. The spectral regions scanned in the instruments from the two manufacturers Picarro and Los Gatos are different (Table 1).

In this work, laser spectrometric isotope and water vapour mixing ratio measurements were performed using two different types of commercial instruments. The Picarro L1115-i (older version) and L2130-i (latest version) isotopic water vapour analysers (Picarro Inc., Sunnyvale, CA, USA) are based on cavity ring-down spectroscopy (Crosson, 2008). The second type of laser system, the water vapour isotope analysers (WVIA and WVIA-EP, DLT-100, version March 2011) by Los Gatos Research Inc. (LGR, Mountain View, CA, USA), are based on off-axis integrated cavity output spectroscopy (Baer et al., 2002). Table 1 summarises the most important properties of the laser systems. The main improvements in terms of measurement quality of the two latest versions of the Picarro and the Los Gatos instruments will be discussed below.

The two systems (L1115-i and WVIA) use laser absorption spectroscopy as a working principle. They however differ in the measured quantity for the derivation of the delta values. In both systems, the sample gas is drawn through an optical cavity, in which pressure and temperature are precisely regulated. Laser light is injected into the cavity through a semi-transparent mirror. A photodetector, placed behind another mirror, measures the light intensity leaking out of the cavity. In the WVIA spectrometer, the optical cavity consists of two slightly astigmatic high reflectivity mirrors and the laser beam is coupled into the cavity in an off-axis alignment. This allows for such a dense mode structure inside the cavity that appears to be always resonant, thus suppressing the need for frequency coupling by adapting the mirror spacing (Paul et al., 2001). In the L1115-i instrument, the cavity is smaller and consists of three mirrors, which are set up in ring configuration. Laser light is injected in alignment with the mirror. In order to obtain cavity frequencies that coincide with the source frequency, the cavity length is adjusted over short distances by a piezoelectric transducer. The laser frequency has to be tightly controlled by a proprietary

wavelength monitor in the L1115-i instrument in order to achieve high spectral resolution (Crosson, 2008). The fitting algorithm for the ring-down technique is time-consuming and is partly responsible for the lower measurement frequency of the L1115-i instrument (Paldus and Kachanov, 2005). Furthermore, pressure and temperature have to be precisely regulated. The technology in the WVIA spectrometer is based on a time-integrated measurement of the radiation intensity leaking out of the cavity, whereas the L1115-i system determines the isotope concentration in the cavity by measuring the exponential ring-down time of the laser intensity after the laser source has been switched off. Ring-down measurements are also done at regular intervals (600 Hz) in the WVIA system, in order to precisely monitor the mirror loss (Doug Baer, personal communication 2012). In the latest version of the Picarro analyser (L2130-i), the spectroscopic fitting algorithm is improved and the data acquisition rate is higher (1 Hz) compared to 0.5 Hz for L1115-i. The WVIA-EP has an improved internal temperature stability.

The tests presented here were done simultaneously for L1115-i, WVIA and WVIA-EP; the same experiments were then repeated for L2130-i later, i.e. at the time this new version of the Picarro water vapour analyser became available.

2.3 Calibration systems

Systematic errors in laser isotope ratio measurements result from drifts due to variations of environmental parameters such as temperature and pressure. In order to correct for such effects and to normalise the isotope measurements with respect to the international reference VSMOW2-SLAP2 scale, the instruments have to be calibrated at regular intervals. Parallel vapour collection in flasks and subsequent reference measurement with IRMS to calibrate the laser instrument is an option suggested by Johnson et al. (2011). However, the normalisation with respect to the international reference scale is indirect in this case and biases introduced by the flask sampling may affect the measurement quality. Direct calibration involves the measurement of a standard vapour sample with known isotopic composition. Calibration standards are generally liquid water standards. Primary international standards are available from IAEA, and referenced working standards are used in the different laboratories worldwide. Direct calibration of a vapour isotope analyser thus involves evaporation of these liquid standards and mixing with a carrier gas before introducing them into the optical cavity for an absorption measurement.

Liquid autosamplers, as used for liquid isotopic laser analyses (see, e.g. Lis et al., 2008), are not optimal for calibrating vapour instruments as the produced calibration vapour quantity is very limited, making extended calibration runs of more than 5 min impracticable. Fractionation effects have to be accounted for if partial evaporation methods are used (Lee et al., 2005; Wen et al., 2008; Wang et al., 2009). For example, with a dew point generator as a calibration system,

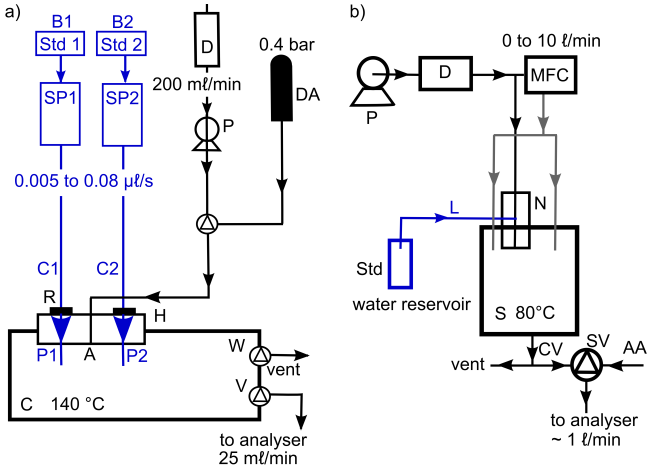

Fig. 1. Flow diagram of the calibration units. **(a)** Standard delivery module (SDM) by Picarro. Std1, Std2: liquid water standards; B1, B2: two collapsible bags for the standards; SP1, SP2: syringe pumps; C1, C2: capillary lines; P1, P2: needle ports; C: vapourisation chamber; A: carrier gas inlet; H: injection head; R: o-rings; P: ambient air pump; D: molecular sieve 5 Å 200 cm^3 with Drierite indicator (Agilent) to dry ambient air as a carrier gas; DA: alternative carrier gas, dry synthetic air (Alphagas, Carbagas); W: waste port of the vapourisation chamber; V: outlet valve leading the calibration air to the measurement cell of the laser instrument. **(b)** The WVISS by LGR. Std: liquid water standard; L: capillary line; N: nebulising system; S: spray chamber; P: ambient air pump; D: drying system containing a regenerative desiccant air dryer and a replaceable Drierite cartridge; MFC mass flow controller for regulating carrier gas flow rate; SV: three-way solenoid valve controlling the vapour source; CV: calibration vapour; AA: ambient air.

dry air is bubbled through a water reservoir at a controlled temperature and the liquid water is continuously enriched in heavy isotopes, following a Rayleigh distillation process. The isotopic composition of the vapour can be determined if the initial and the residual water isotopic composition are known and if the temperature in the water reservoir is precisely regulated or measured. Calibration techniques allowing complete evaporation of the liquid standards operate by continuously dripping liquid droplets into a dry air stream using a syringe pump or a capillary dripping system as proposed by Iannone et al. (2009) and used in a slightly altered setup by Sturm and Knohl (2010). Similar techniques are used in the commercial calibration systems for water vapour isotope measurements from Picarro and Los Gatos, which have become available recently and are used in this study.

The commercial calibration system for the L1115-i instrument comprises a vapouriser and a standard delivery module A0101 (SDM; see Fig. 1a). This calibration system allows for the automated use of two liquid standards in parallel (Std1 and Std2 in Fig. 1a). The standards are filled into collapsible bags (B1, B2). The liquid standards are then pumped by syringe pumps (SP1, SP2) via capillary lines (C1, C2) to

the injection head (H) of the vapouriser. The injection system consists of two needle ports (P1, P2) and a carrier gas inlet (A). The head of the needles penetrates the vapourisation chamber (C), the temperature of which is regulated at 140 °C to ensure immediate and full evaporation of the liquid standard introduced through the needles. The needle port is sealed with three o-rings (R) to avoid ambient air penetration into the vapourisation chamber when no calibration is done, and to prevent leaking of dry air during calibration. When a calibration run is performed, the liquid standards are pumped into the vapouriser and a constant dry air flow sustains immediate evaporation of the liquid in the air stream. The dry air, serving as a carrier gas, is pumped at a rate of 200 ml min^{-1} through a molecular sieve 5Å MT-D 200 cm^3 (D) with Drierite indicator (Agilent) into the vapouriser. Alternatively, dry synthetic air (Alphagas synthetic air, Carbagas, $H_2O < 3\,\mu mol\,mol^{-1}$, $C_nH_m < 0.5\,\mu mol\,mol^{-1}$, $O_2 = 20\,\% \pm 1\,\%$) was used at an over-pressure of 0.4 bar (DA) (see Sect. 5), while the dry air pump was switched off. The waste port valve (W) of the vapouriser is constantly opened in order to establish a steady flow through the vapourising chamber. To exclude memory effects from the previous calibration run and to allow reaching moist air equilibrium in the vapouriser, the outlet valve (V) of the vapouriser to the measurement cell is switched open only after a delay of five minutes. The water vapour mixing ratio of the calibration gas can be varied in the range 2000–30 000 ppmv by controlling the liquid pumping rate between 0.005 µl s^{-1} and 0.08 µl s^{-1}.

The central element of the water vapour isotope standard source (WVISS, Fig. 1b) by Los Gatos Research is a nebulising system (N) guiding a capillary inlet line (L), which serves as a dripping system into a 1 L spray chamber (S) heated to 80 °C. Ambient air is pumped through a two-stage drying system (D) containing a regenerative desiccant air dryer and a replaceable Drierite cartridge. The water vapour mixing ratio can be regulated via a mass flow controller (MFC), which adjusts the dry air flow rate (0–10 l min^{-1}). This way water vapour mixing ratios in the range 5000–30 000 ppmv can be produced. A three-way solenoid valve (SV) controls the vapour source, which is either the calibration vapour (CV) or ambient air (AA). The system allows only for one automated liquid standard (Std) to be measured when calibration is unattended. In addition to producing only one vapour standard, the disadvantage of the LGR calibration system is its bulkiness (Table 1), which complicates field work. However, in contrast to the Picarro system, it allows for stable production of large quantities of calibration vapour over several days. Therefore, in the experiments conducted in this study, the WVISS was used to measure the same standard in parallel with the Picarro and LGR instruments.

In the following sections, the colour coding for the results is blue for the measurements by the Picarro instruments and red for the measurements by the Los Gatos instruments.

Table 2. Isotopic composition (in ‰) of the international IAEA standards and working standards (WS) used for the characterisation of the laser systems. The indicated isotopic δ values of working standards 1–10 were measured with IRMS.

Standard	IRMS	
name	δ^2H [‰]	δ^{18}O [‰]
IAEA VSMOW2	0 ± 0.30*	0 ± 0.02*
IAEA SLAP2	-427.50 ± 0.30*	-55.50 ± 0.02*
IAEA GISP2	-189.50 ± 1.20*	-24.76 ± 0.09*
WS 1	-107.32 ± 1.10	-14.35 ± 0.04
WS 2	-140.03 ± 1.93	-18.42 ± 0.10
WS 3	-172.52 ± 1.11	21.46 ± 0.14
WS 4	-79.29 ± 0.62	-5.24 ± 0.25
WS 5	-188.13 ± 1.57	-24.72 ± 0.14
WS 6	-78.68 ± 0.19	-10.99 ± 0.12
WS 7	-153.90 ± 1.06	-24.89 ± 0.73
WS 8	-256.11 ± 0.85	-46.02 ± 0.82
WS 9	-166.74 ± 0.35	-70.19 ± 2.74
WS 10	14.89 ± 0.61	3.63 ± 0.35

* IAEA standard composition as stated in IAEA (2009).

3 Delta scale linearity

The focus of this first experiment was to verify the linearity of the calibrated laser spectroscopic measurements in the VSMOW2-SLAP2 range of the isotope delta scale with an independent measurement technique. Ten working standards (WS 1–10, Table 2) were measured with both laser instruments and the WVISS calibration unit for 10 min, each at a water vapour mixing ratio of 18 000 ppmv. The first two minutes and the last minute of each calibration run were discarded to account for the purging time of the lines. All measurements were done twice (run 1 and run 2), each time within a day. Furthermore, between two working standard calibration runs, we measured a drift standard for three minutes in order to remove memory effects from the calibration unit and to monitor the behaviour of the measurement system over the whole calibration experiment.

The standards measured with the two laser spectrometers were compared to IRMS measurements, done on a Delta^{PLUS}XP mass spectrometer (Thermo Fisher Scientific Inc., Germany) using a high-temperature conversion/elemental analyser coupled on-line to the mass spectrometer via a ConFlo III interface (Gehre et al., 2004).

Both measurements using IRMS and laser spectroscopy were calibrated and normalised to the VSMOW2-SLAP2 scale (IAEA, 2009) using the IAEA standards VSMOW2 and SLAP2 directly. This procedure was chosen because VSMOW2 and SLAP2 span the whole δ scale range of our standards, and it provides a way to independently calibrate our working standard measurements. For daily calibration purposes, our internal standards are used as recommended in IAEA (2009), i.e. not the IAEA standards.

Table 3. Results from the delta-scale linearity experiment. The two laser systems L1115-i and WVIA were compared to IRMS using ten standards, which were measured on all the instruments twice (run 1 and run 2). The average differences over the ten standards for the different instrument combinations are listed. $\overline{\sigma_s}$ indicates the average standard deviation of the measurements over all working standard runs. The standard deviation of the drift standard measurements over the individual runs was 1.2 ‰ (0.7‰) for δ^2H of L1115-i (WVIA) and 0.3 ‰ (0.3‰) for δ^{18}O of L1115-i (WVIA).

Instrument combination	δ^2H [‰]	δ^{18}O [‰]
(a) L1115-i vs. WVIA	0.8 ± 0.9	0.4 ± 0.5
(b) L1115-i vs. IRMS	0.7 ± 0.8	0.1 ± 0.1
(c) WVIA vs. IRMS	0.5 ± 0.6	0.1 ± 1.3
(d) L1115-i 1 vs. L1115-i 2	1.9 ± 1.6	0.2 ± 0.2
(e) WVIA 1 vs. WVIA 2	0.8 ± 0.6	0.2 ± 0.2
(f) L1115-i $\overline{\sigma_s}$	1.7 ± 0.4	0.5 ± 0.1
(g) WVIA $\overline{\sigma_s}$	1.0 ± 0.2	0.4 ± 0.1
(h) IRMS $\overline{\sigma_s}$	0.5 ± 0.1	0.09 ± 0.04

All calibrated laser spectroscopy measurements are in very good agreement with the calibrated IRMS values ($R^2 > 0.99$ for both isotopes, Fig. 2). The largest differences between the laser measurements and IRMS occur at the edge of the δ scale.

WS 1–10 were measured twice with the two laser systems, and the average differences between the two runs 1 and 2 over all standards are below 1 ‰ for both isotopes and both instruments, except for the δ^2H of the L1115-i instrument (Table 3d, e). This surprisingly high δ^2H uncertainty in the L1115-i measurements is also reflected in the average standard deviation of the calibration runs over all standard measurements (Table 3f) and is probably due to memory effects in the instrument during the measurement of the standards. Memory effects can be characterised by the typical response time of an instrument to a step change of the input signal. The L1115-i has much longer response times than WVIA (as will be discussed in Sect. 7 below). Furthermore, the memory effects are more important for δ^2H than for δ^{18}O, which may explain the significantly higher uncertainty obtained here for the δ^2H signal of L1115-i.

The inter-comparison of the calibrated standard values obtained from the different instruments shows average deviations in the range 0.5–0.8 ‰ in δ^2H and in the range 0.1–0.4 ‰ in δ^{18}O (Table 3a–c). These values are equivalent to the average standard deviation over all the samples measured with the different instruments (Table 3f–h), except the already discussed high δ^2H uncertainty of the L1115-i. The standard deviation of the drift runs is 1.2 ‰ for δ^2H of L1115-i, 0.7 ‰ for δ^2H of WVIA and 0.3 ‰ for δ^{18}O of both instruments. These values are in the order of the uncertainties of the measurement systems quantified in Table 3.

For the ten samples measured here, the average standard deviations of the IRMS measurements are $\sigma(\delta^2\text{H})$=0.5 ‰ and $\sigma(\delta^{18}\text{O})$=0.09 ‰ (Table 3). These values do not include any sampling uncertainty (e.g. cryogenic trapping of a water vapour sample for later analysis). The laser spectroscopic measurements however include sampling uncertainties in this experimental setup and are characterised by only slightly higher standard deviations (except for the much higher δ^2H uncertainty of L1115-i).

The uncertainties of the isotope standard measurements with the two laser spectroscopic systems obtained from error propagation after calibration depend on the δ value of the chosen calibration standard (Fig. 3). The dominant uncertainty component is the error associated with the laser measurement of the two calibration standards. The error contribution of the laser measurement of standard 1 is highest around the δ value of this standard (here 0‰) and decreases with increasing difference to its δ value (here decreasing δ values). The error contribution of the laser measurement of standard 2 shows a similar behaviour, symmetric to the error contribution of standard 1, which leads to the "U-shaped" dependency on the δ value of the total sample measurement uncertainty. The larger uncertainties of L1115-i standard measurements (blue crosses) compared to WVIA (red crosses) are due to the lower short-term precision of the instrument (Sect. 6.1) and to the longer response time characteristics (Sect. 7), which introduce larger memory effects than for WVIA.

An important aspect of the calibration strategy of a laser spectroscopic instrument is whether a two-point calibration is necessary or a one point calibration (only bias correction) is sufficient. The calibration system WVISS only allows for automatic measurements using one standard. To investigate this aspect, we computed the normalisation factors and their uncertainty following IAEA (2009) for the two calibration runs (Table 4). For L1115-i the normalisation factors as well as the intercepts were different in the two runs. In the case of δ^2H, the change in the zero point was large with a difference of 11 ‰. For WVIA we found that the normalisation factors remained within the uncertainty range; the intercept however changed slightly. As L1115-i, WVIA and WVIA-EP were connected to the WVISS in parallel, the large change in the δ^2H signal calibration factors of the L1115-i must come from the instrument itself. This might indicate that regular two-point calibration is necessary for L1115-i and that one standard might be sufficient for WVIA calibration, but further investigation with more calibration runs would be needed to confirm this preliminary finding.

4 Water vapour mixing ratio calibration

For the investigation of the water vapour concentration dependency of isotope measurements, the water vapour mixing ratio data of the two instruments had to be calibrated. A dew

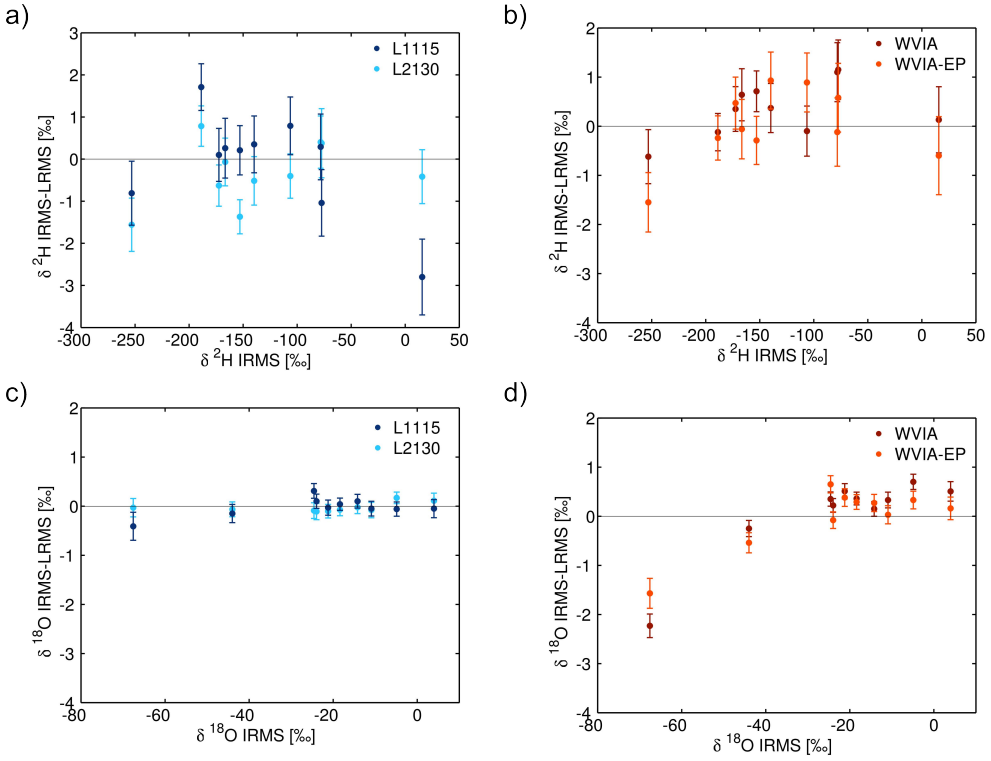

Fig. 2. Difference between the laser instrument measurements (LRMS) and IRMS for **(a)** δ^2H of L1115-i and L2130-i, **(b)** δ^2H of WVIA and WVIA-EP, **(c)** δ^{18}O of L1115-i and L2130-i, **(d)** δ^{18}O of WVIA and WVIA-EP measurements for the ten WS 1–10 (Table 2).

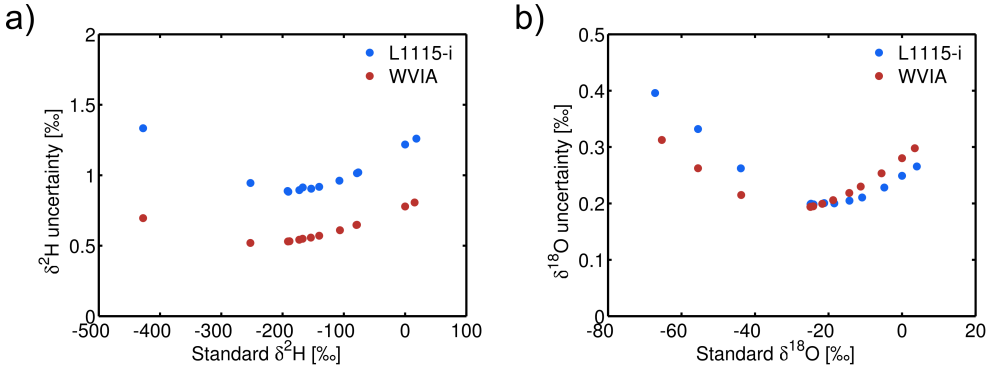

Fig. 3. Uncertainty of **(a)** δ^2H and **(b)** δ^{18}O isotope calibration runs by L1115-i and WVIA as a function of isotopic composition of the WS 1–10 as well as the IAEA standards (Table 2).

Table 4. Uncertainty in calibration factors following IAEA (2009). The normalisation slopes for both isotopes were determined for two calibration runs 1 ($f1$) and 2 ($f2$) using VSMOW2 and SLAP2 as reference standards. The intercepts of the calibrations from the two runs ($b1$) and ($b2$) are the measured VSMOW2 raw values of the laser instruments.

Calibration factors	L1115-i		WVIA	
	δ^2H	δ^{18}O	δ^2H	δ^{18}O
$f1$ [–]	1.064 ± 0.009	1.113 ± 0.008	0.995 ± 0.003	0.939 ± 0.009
$f2$ [–]	0.995 ± 0.004	1.029 ± 0.007	0.994 ± 0.002	0.942 ± 0.006
$b1$ [‰]	-9.0 ± 1.9	-15.2 ± 0.2	0.4 ± 1.0	4.5 ± 0.4
$b2$ [‰]	2.1 ± 1.2	-14.1 ± 0.2	0.7 ± 0.8	3.0 ± 0.3

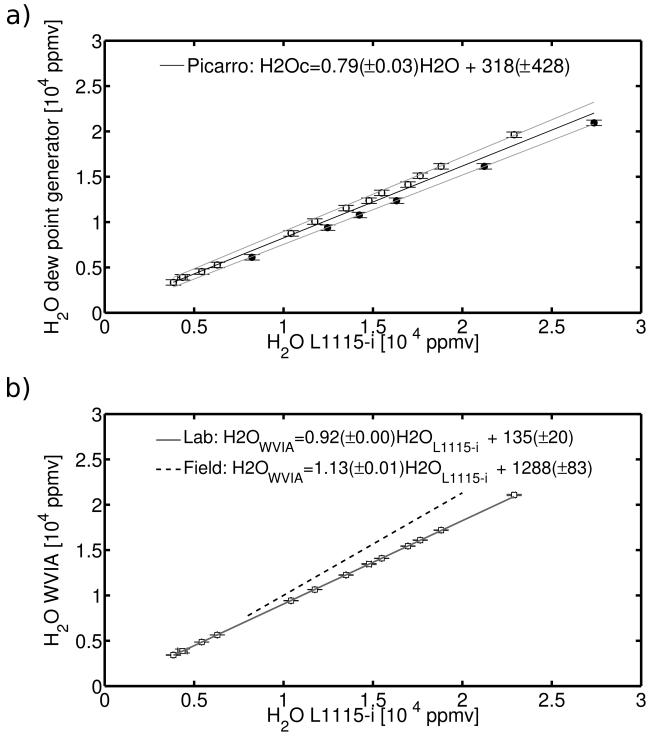

Fig. 4. Calibration of water vapour mixing ratio measurements. **(a)** L1115-i laboratory calibration measurements. The calibration experiment with the dew point generator was done twice: once with L1115-i connected to the LI-610 alone (full circles) and once with L1115-i and WVIA connected in parallel to the LI-610 (open squares). A least squares fit to all data points of the two experiments is shown by the black line. The grey lines show the standard deviation of the least square fit. In **(b)** WVIA and L1115-i measurements are compared using parallel laboratory measurements (grey line) and parallel field measurements (black dashed line). The laboratory data points (black squares) show average measured water concentration of hourly runs and their standard deviation. The grey line represents a least square fit to the laboratory data points. The black dashed line represents the least square fit to the ambient air measurements. The uncertainty of these fits is very small and thus not shown.

point generator (LI-610, LI-COR Inc., Lincoln, NE, USA) was used for this purpose. Two water vapour mixing ratio calibration series were performed. In one of these two runs, both instruments were connected in parallel to the dew point generator and measured water vapour mixing ratios simultaneously from the same source. Another run was performed with only the L1115-i instrument connected to the LI-610. Mixing ratios between 3000 and 30 000 ppmv were produced in a constant flow of $1\,\mathrm{l\,min^{-1}}$ of moist air with an uncertainty of ∼100–400 ppmv (increasing for larger dew point temperatures). Calibration runs always lasted for at least 2 h for each dew point temperature: 1 h for equilibration of the air flow through the water reservoir in the dew point generator and 1 h of measurements considered in the data analysis. The calibration functions determined from the laboratory experiments were then used in order to calibrate the data of each instrument. To verify the parallel water vapour mixing ratio calibration experiment from the laboratory, ambient measurements of water vapour mixing ratio were performed in parallel in a field setup as described in Sect. 8.

The measurement range of the water vapour mixing ratio specified by the two manufacturers is between 5000 and 30 000 ppmv, which was well covered by our water vapour mixing ratio calibration measurements. The water vapour mixing ratios measured by the L1115-i and the WVIA instruments both show a linear relationship with the theoretical dew point generator values over the whole measurement range as can be seen from the calibration line of L1115-i in Fig. 4a and the grey line in Fig. 4b, which illustrates the correspondence of the L1115-i and the WVIA values. The calibration lines obtained here for water vapour mixing ratio for the two instruments are the following:

$$\mathrm{H_2O_{L1115\text{-}i,cal}} = 0.79 \cdot \mathrm{H_2O_{L1115\text{-}i,m}} + 318\ \mathrm{ppmv} \quad (2)$$

$$\mathrm{H_2O_{WVIA,cal}} = 0.92 \cdot \mathrm{H_2O_{WVIA,m}} + 117\ \mathrm{ppmv} \quad (3)$$

The water vapour mixing ratio calibration procedure using a dew point generator is time-consuming and lasts for several days due to the long equilibration and measurement times. It can thus not be repeated regularly without a major loss of ambient measurement time. The error associated with using the same calibration parameters for the water vapour mixing ratio during a measurement campaign can be quantified

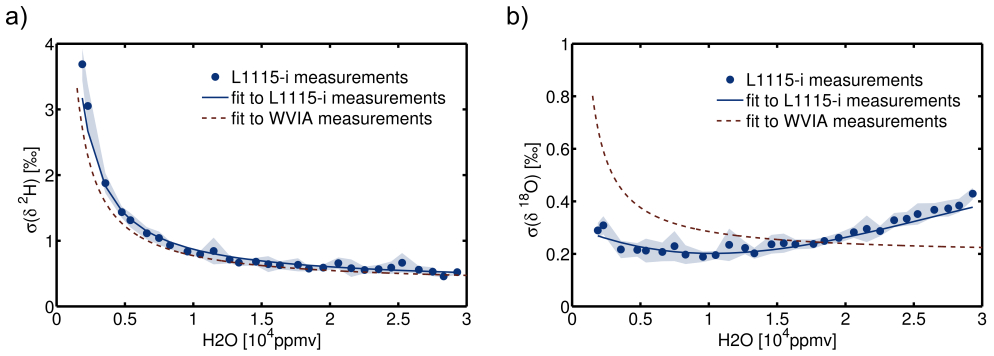

Fig. 5. Dependency of the δ^2H **(a)** and δ^{18}O **(b)** measurement precision (average standard deviation σ of calibration runs) on water vapour mixing ratio for L1115-i (solid lines and data points). The fit to the WVIA measurements (dashed lines) found by Sturm and Knohl (2010) is shown for comparison. The shading represents the standard deviation of all calibration runs with four different standards (WS 6–9 in Table 2).

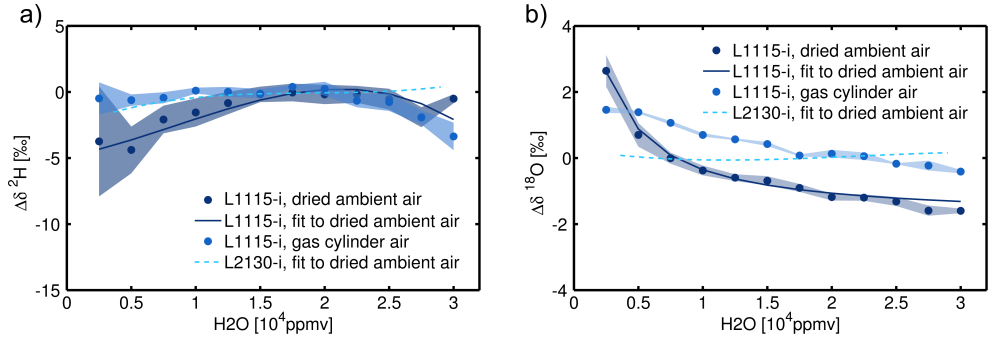

Fig. 6. Dependency of the L1115-i isotope measurements on water vapour mixing ratio for δ^2H in **(a)** and δ^{18}O in **(b)**. The data were calibrated independently using the WVISS calibration unit and the IAEA standards VSMOW2 and SLAP2 at a water vapour mixing ratio of 18 000 ppmv. The shading represents the standard deviation of all calibration runs with four different working standards (WS 6–9 in Table 2). The full blue curves are least square fits to the data obtained using dried ambient air as a carrier gas. The dashed curves show least square third order polynomial fits to the L2130-i measurements.

by the standard error of the calibration fitting in Fig. 4a, for which data from two independent calibration runs (full circles and white squares) were used. The water vapour mixing ratio uncertainty resulting from the calibration parameters thus amounts to ∼400 ppmv. Compared to the parallel laboratory run with the dew point generator (white squares and grey line in Fig. 4b), the parallel field run (blue line in Fig. 4b) shows a larger spread (85 ppmv standard error for the field measurements vs. 20 ppmv standard error for the lab measurements) and a bias (∼ 1300 ppmv) with respect to the laboratory correspondence line. This indicates that the measurement uncertainty in field measurements is higher than what could be quantified under controlled conditions in the laboratory. Effects from the sampling lines (material and length) may play a role in this higher uncertainty. The bias with respect to the laboratory correspondence line indicates a need for more frequent water vapour mixing ratio calibration than just sporadic laboratory calibrations if accurate water vapour mixing ratios are required.

For the remainder of this study, we adopted the calibration lines obtained from the laboratory calibration run to correct water vapour mixing ratios and used results from the parallel field run as an uncertainty estimate.

5 Water vapour mixing ratio dependency of isotope measurements

The spectroscopic measurements of water vapour isotopes are affected by the water vapour mixing ratio in two ways. First, the precision of the measurement depends on the water vapour mixing ratio. Second, the isotope measurement is affected by a bias, which depends on water vapour mixing ratio. Both aspects were already discussed by Sturm and Knohl (2010) for the WVIA instrument. Hence, they are investigated here only for the L1115-i and the L2130-i systems. Because water vapour mixing ratio effects directly affect calibration, we tested the water vapour mixing ratio dependency of the L1115-i system using the SDM. Furthermore, this is the setup we used during the comparative field experiment

(Sect. 8). Four calibration runs were performed in steps of 1000 ppmv in the range 2000–30 000 ppmv using four different standards (WS 6–9, Table 2). Calibration runs lasted for 20 min each. Depending on the type of carrier gas used, interfering effects can influence the calibration gas measurements. For example, remaining ambient water vapour when using dry cells can change the isotopic values of the standard. Furthermore, traces of other gases also absorbing laser light in the same spectral domain can affect the measurements. To investigate the effect of the carrier gas source, two different carrier gases were compared: (1) synthetic dry air from a gas cylinder and (2) dried ambient air using a molecular sieve with indicating Drierite (Sect. 2.3). The calibration runs for each standard were done twice in blocks of approximately one day. The carrier gas sources were alternated. The data were calibrated independently using the WVISS calibration unit and the IAEA standards VSMOW2 and SLAP2 at a water vapour mixing ratio of 18 000 ppmv. The concentration dependency of the L2130-i was tested using the WVISS with dry ambient air as a carrier gas and only WS 6. The SDM was not available when the experiments with L2130-i were performed.

5.1 Dependency of the isotope measurement precision on water vapour mixing ratio

The measurement precision of δ^2H for the L1115-i instrument improves with increasing water vapour mixing ratio (Fig. 5a). This finding concurs with a higher signal-to-noise ratio for a larger number of molecules and is similar to the one found by Sturm and Knohl (2010) for WVIA. The δ^{18}O precision however exhibits a different behaviour (Fig. 5b): The precision of δ^{18}O improves with augmenting water vapour mixing ratios at very low water vapour mixing ratios, up to around 8000 ppmv, where it reaches a maximum. For water vapour mixing ratios above 8000 ppmv, the precision of δ^{18}O deteriorates again. This can be understood by considering the absorption spectrum. The absorption peak of δ^{18}O is stronger than the one of δ^2H (Kerstel et al., 2002; Gianfrani et al., 2003; Rothman et al., 2009). Thus, in the case of δ^{18}O the sensitivity of the measurement can be affected by optical saturation at much lower water concentration values than in the case of δ^2H (Gregor Hsiao, Picarro, personal communication, 2011). The water vapour mixing ratio dependency of δ^{18}O for WVIA found in Sturm and Knohl (2010) and the results obtained for the new version L2130-i do not show such an optical saturation effect. For the WVIA the water vapour mixing ratio dependency is stronger in amplitude for δ^{18}O compared to our results for L1115-i (as shown by the dashed lines in Fig. 5). For δ^2H the water vapour mixing ratio dependency of WVIA is practically identical to what is found here for L1115-i. With the new version L2130-i, the precision is comparable, or even slightly better than in L1115-i (Table 5).

Table 5. Standard deviation of laser spectroscopic isotope measurements at 5000 ppmv and 20 000 ppmv water vapour mixing ratio.

Instrument	δ^2H [‰]		δ^{18}O [‰]	
	at 5000 ppmv	at 20 000 ppmv	at 5000 ppmv	at 20 000 ppmv
L1115-i	1.3	0.6	0.22	0.25
L2130-i	1.1	0.4	0.25	0.19
WVIA	1.2	0.6	0.38	0.22

5.2 Dependency of the isotope measurement accuracy on water vapour mixing ratio

The average per mil deviations ($\Delta\delta^2$H and $\Delta\delta^{18}$O) expressed with respect to the calibrated isotope values of the four standards at 18 000 ppmv are shown in Fig. 6 as a function of water vapour mixing ratio for the L1115-i instrument. The dark blue dots (Fig. 6a, b) show the average isotope measurement bias dependency of water vapour mixing ratio using dried ambient air as a carrier gas. The standard deviation of the different runs performed in the corresponding water vapour mixing ratio range is represented by the shaded domain in Fig. 6. Biasing effects of up to 4 ‰ for δ^2H and 2.5 ‰ for δ^{18}O (Fig. 6a, b) due to varying amounts of water vapour in the gas samples can be observed with the L1115-i instrument. These dependencies on water vapour mixing ratio are considerable compared to the precision of the instrument (see Sect. 6), and they should be corrected especially when measurements are performed at a field site where water vapour mixing ratio can vary strongly (>1000 ppmv in 12 h in Johnson et al. (2011)). For L1115-i we use the following least square fits represented by the dark blue curves in Fig. 6:

$$\Delta\delta^2\mathrm{H} = -6.4\times10^{-13}[\mathrm{H_2O}]^3 + 1.6\times10^{-8}[\mathrm{H_2O}]^2 + 1.9\times10^{-4}[\mathrm{H_2O}] - 4.9 \quad (4)$$

$$\Delta\delta^{18}\mathrm{O} = \frac{-1.2\times10^{7}}{[\mathrm{H_2O}]^2} + \frac{1.6\times10^{4}}{[\mathrm{H_2O}]} - 1.8 \quad (5)$$

Fig. 6 shows the uncertainty range of these corrections. This uncertainty of the water vapour mixing ratio correction propagates into the isotope measurement uncertainty. Similar dependencies were found by Schmidt et al. (2010) for the L1102-i version of the water vapour isotope instrument by Picarro. Since the correction can be different for every instrument, this characterisation step has to be done individually for every instrument. Rambo et al. (2011) found that this dependency on water vapour mixing ratio varies significantly in time for WVIA. In our case the dependency remained similar in terms of amplitude and shape when the experiment was repeated at a later time. However, regular calibration of the instrument at different water vapour mixing ratios spanning

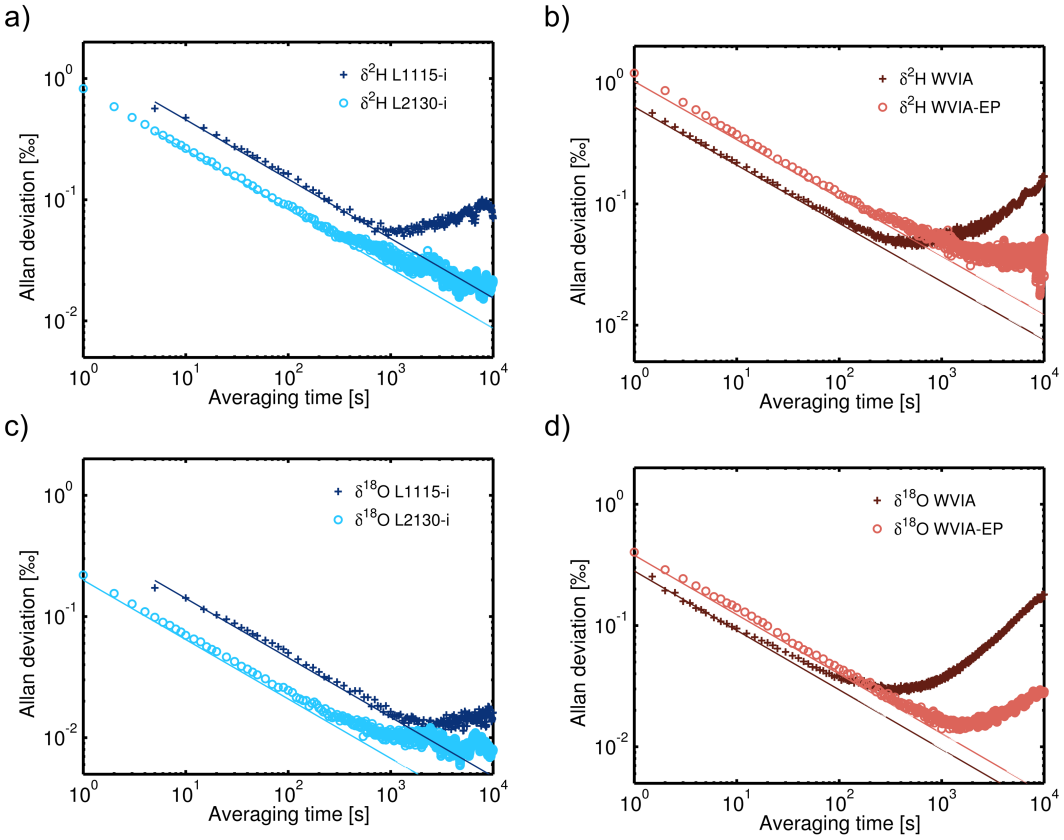

Fig. 7. Short-term stability of δ^2H (**a** and **b**) and δ^{18}O measurements (**c** and **d**) at 15 700 ppmv water vapour mixing ratio by L1115-i/L2130-i (**a** and **c**) and WVIA/WVIA-EP (**b** and **d**). The square root of the Allan variance is shown as a function of aggregation time on a log-log scale. The solid lines show the expected behaviour of a pure white noise signal with the same variance as the measured signal at the time scale of data acquisition (5 s for L1115-i and 1 s for WVIA, WVIA-EP, L2130-i).

the ambient air measurements is necessary to ensure that the bias is correctly removed.

The changing bias in the isotope measurements as a function of water vapour mixing ratio is probably due to non-linearities in the spectroscopy and uncertainties in the spectral fitting algorithm (Gupta et al., 2009). Variations in water vapour mixing ratios also affect the spectral baseline, thus altering the fitting of the absorption measurements to the theoretical spectral lines.

For the new version L2130-i of the Picarro instrument, much smaller dependencies on the water vapour mixing ratio were found (Fig. 6, dashed lines). A water vapour mixing ratio correction for L2130-i may only be necessary if water vapour isotope samples in strongly varying water vapour mixing ratio conditions are taken, including some samples at very low water vapour mixing ratios. However, for the old versions of the Picarro instrument, water vapour mixing ratio-dependent bias corrections are indispensable.

The bias dependencies on water vapour mixing ratios are different for the two tested carrier gases in the case of δ^{18}O and more similar for δ^2H (Fig. 6a, b; light and dark curves). The observed discrepancy in the δ^{18}O bias may be due to changes in the baseline of the spectrum around the δ^{18}O absorption peak, caused by slight differences in trace gas composition. Effects due to hydrocarbons or different CO_2 composition can be excluded, since filtering ambient air with a CO_2 absorber and a hydrocarbon trap did not remove the difference between the measurements. However, the effect of methane cannot be excluded and is known to be an important interfering species especially at low water vapour mixing ratios (Hendry et al., 2011). In the case of δ^2H, the measured dependencies diverge only at very low water vapour mixing ratios, especially due to the large uncertainties in the curve found for the dried ambient air as carrier gas (Fig. 6a). Generally, the standard deviation of the bias in isotope measurements is smaller when gas cylinder air is used. In the case of the dried ambient air, the residual humidity is much higher (∼100 ppmv) than in the dry synthetic air (∼30 ppmv). The latter is only affected by memory effects from the walls of the tubing and the cavity. In the dried ambient air, however, the background water vapour mixing ratio influences the isotopic composition of the measured sample significantly at low water vapour mixing ratios. This results in a higher variability of the measurements especially at low water vapour mixing

ratios. In principle, the effect of remaining ambient water vapour in the carrier gas can be corrected. However, for such a correction a good estimate of the true isotopic composition of the carrier gas is needed, which is difficult to obtain due to the high uncertainty of isotopic measurements at very low water vapour mixing ratios, especially for δ^2H (Fig. 5). We estimated the isotopic composition of dried ambient air by performing calibration runs without pumping any liquid into the vapouriser. We found $\delta^2H_{\,dry} = (-293 \pm 45)$ ‰ and $\delta^{18}O_{dry} = (-47 \pm 2)$‰. Due to these high uncertainties in the estimation of dried ambient air isotopic composition, a correction for remaining ambient water vapour just introduces a higher uncertainty at low water vapour mixing ratios and is not useful to get a better water vapour dependency correction function. Even though using dried ambient air as a carrier gas implies the problem of residual ambient humidity, we use it for calibration in the field rather than air from a gas cylinder, because its composition in terms of other trace gases is the same as for the sample gas measured.

6 Stability of water vapour isotope measurements

The stability of a laser spectroscopic system is an important characteristic, which allows to quantify the precision of the measurement system for given averaging times, the instrument internal drifts as well as the optimal calibration time. In this section we investigate the effects of drift and choice of calibration time on precision and accuracy of the isotope measurements in two different experiments. First, we present the results from a stability test performed at the timescale of 1 day (Sect. 6.1). Then, we discuss a slightly different experiment that was designed to analyse stability over a period of 14 days (Sect. 6.2).

6.1 Short-term stability

Short-term stability was tested by measuring WS 6 (Table 2) at a water vapour mixing ratio of 15 700 ppmv over 24 h. An Allan variance analysis was then performed using the measured δ^2H and δ^{18}O time series in order to get a quantitative estimate of the precision of the signals at different aggregation time scales.

Introduced by Allan (1966) and presented by Werle (2011) as a general method to characterise the stability of tunable diode laser absorption spectrometers, the Allan plot is a useful tool to analyse the precision and the drift components of such a measurement system. The Allan variance measures the difference between two consecutive signal values y_i and y_{i+1} at a given aggregation time scale τ averaged over the total number of averaging intervals n:

$$\sigma_A^2(\tau) = \frac{1}{2n}\sum_{i=1}^{n}(y_{i+1}(\tau) - y_i(\tau))^2. \quad (6)$$

The short-term stability of the constant isotope signal in Fig. 7 is expressed in terms of the square root of the Allan variance, the Allan deviation as a function of averaging time. Consider, for example, the Allan plot for δ^2H of L1115-i (dark blue crosses in Fig. 7a). The Allan deviation decreases towards higher averaging times up to a minimum, which is at the optimum averaging time ($\tau_0 = 10^3$ s) and then increases again for averaging times $> \tau_0$. These two stability domains, which are separated by the minimum of $\sigma_A(\tau)$ at τ_0, can be observed in all the Allan curves of Fig. 7. The left side shows increasing precision with longer averaging times. This corresponds to statistically independent measurements with a white frequency spectrum, as shown by the solid line. The latter is obtained from Allan deviations computed from a randomly generated white noise signal with the same variance as the measurements at the temporal resolution of the data acquisition. In theory, infinite averaging would thus lead to a perfectly stable system (Werle, 2011). In real systems, however, a minimum is reached at the optimum averaging time, after which the averaged signal is dominated by instrument drift. These drifts are due to low frequency variations in controlling elements of the spectrometer like temperature, pressure, laser current or varying environmental conditions, or due to slight changes in the properties of the calibration vapour.

The key characteristics of the Allan plot of the four investigated laser instruments such as the optimal integration time (τ_0), the Allan deviation at optimal integration time ($\sigma_A^{\tau_0}$) as well as the Allan deviation at high temporal resolution (σ_A^{5s}) are summarised in Table 6. For mesoscale meteorological applications, an averaging time range of 15 min to 6 h is useful, and thus precision values as indicated in Table 6 for $\sigma_A^{\tau_0}$ can be expected. Natural variations in water vapour isotopic composition associated with mesoscale meteorological weather systems are much larger than the precision values and drift amplitude obtained here (see Sect. 8). The precision of the WVIA is slightly higher than the one of the L1115-i instrument at small integration times. However, the minimum Allan deviation is reached later by the L1115-i signal, and at integration times >20 min stability is better, in particular for δ^{18}O. The stability performance of the WVIA found here is similar to the results by Sturm and Knohl (2010). The latest versions of the two instruments (L2130-i and WVIA-EP) show better performance in terms of precision. The L2130-i instrument has smaller Allan deviations than the L1115-i for all integration times and longer optimal integration times. The precision of the WVIA-EP is not improved with respect to WVIA for small integration times; however, it is characterised by larger optimal averaging times and reaches higher precision than WVIA at longer integration times.

6.2 Long-term stability

A stability analysis for time scales of several days was conducted as a complement to the short-term stability test to

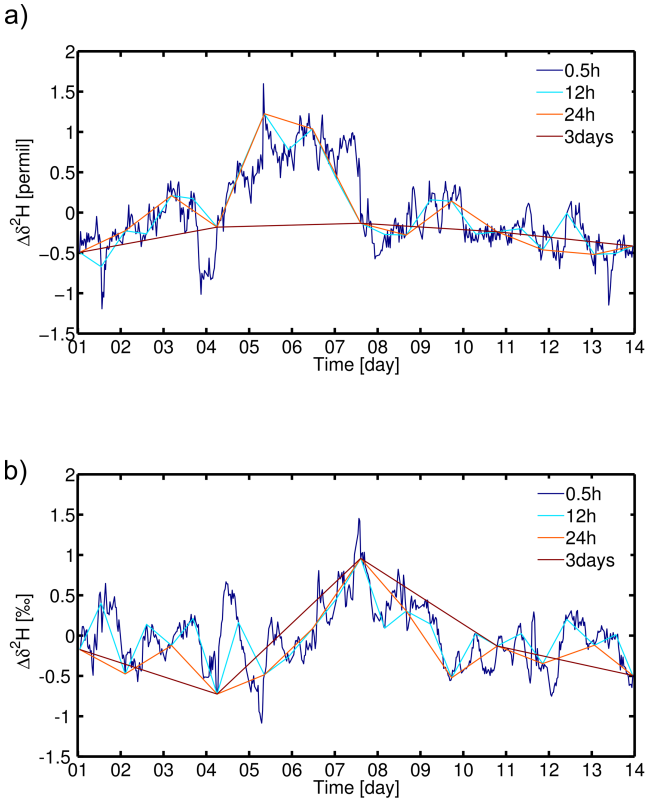

Fig. 8. Temporal evolution of the bias correction amplitude of isotope measurements with L1115-i **(a)** and WVIA **(b)** at 15 700 ppmv water vapour mixing ratio over 14 days. Each line corresponds to one calibration frequency scheme. The dark blue correction curve is obtained if the instrument is calibrated every 30 min.

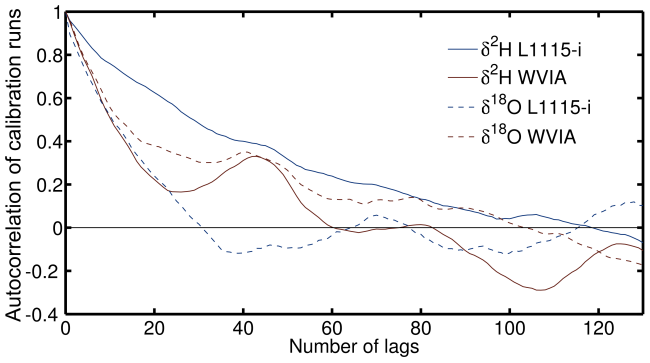

Fig. 9. Autocorrelation function of the isotopic composition of the calibration runs of the long-term stability experiment for L1115-i and WVIA. A lag of 1 corresponds to a 30 min calibration interval.

investigate changes in the instrument calibration at the time scale >1 day and as complementary information for finding the ideal calibration scheme. Long-term stability was investigated by measuring WS 6 at regular intervals of 30 min for a duration of 10 min. During the remaining 20 min ambient air was measured. This regular calibration sequence was performed over 14 days. The first two minutes and the last minute of each calibration run were discarded for the data analysis to avoid biases due to non-steady state effects.

The long-term stability of the δ^{18}O and δ^{2}H calibration time series of both instruments was assessed by applying a bias correction, which was calculated for varying calibration intervals. Because only one standard was measured here, the calibration consists of a simple bias correction. The bias correction was computed by linearly interpolating between two consecutive calibration runs. This procedure is illustrated for the δ^{2}H signal in Fig. 8a and b for L1115-i and WVIA, respectively. Here, the colour coding refers to the calibration interval and not to the instrument type. Sub-daily calibration (light blue curve in Fig. 8) allows to correct drifts more accurately than if calibration is only done every few days (dark red curve in Fig. 8). The maximum amplitude of the corrections is rather small with ~ 1 ‰ for δ^{2}H and ~ 0.5 ‰ for δ^{18}O. These bias correction amplitudes may be larger for δ values at the edge of the VSMOW-SLAP scale. The long-term stability experiment was only done with WS6 at δ^{2}H = −78.68 ‰, but the results shown in Table 4 (compare the intercepts $b1$ and $b2$ for L1115-i) and discussed in Sect. 3 suggest that changes of up to 10 ‰ in the measurement bias can occur over several days at δ^{2}H =0‰.

The observed drifts in both L1115-i and WVIA are due to low frequency changes in instrument characteristics. They can be limited by applying regular calibration. In this experiment artificial drifting effects introduced by the calibration system itself cannot be excluded. However, the bias correction time series of the two instruments are uncorrelated (Fig. 8a, b), which is a good indication that instrument drifts prevail over the calibration system drifts.

A certain memory in the amplitude and sign of the bias correction time series for both instruments (Fig. 8a, b) can be observed. To find out for how long on average a given bias correction is still useful, the autocorrelation functions of the time series of the calibration runs were computed and are shown in Fig. 9. The minimum number of lags at which the autocorrelation function of the isotope signal of a given instrument reaches zero gives an indication about the maximum time range of validity of a bias correction. For the L1115-i δ^{18}O and δ^{2}H signals, it is 15 h and 2.5 days, respectively. For the WVIA the values are 2 days and 1.5 days for the δ^{2}H and δ^{18}O signals, respectively. Inter-calibration periods longer than these durations do not improve the measurements.

A second characteristic of the calibration scheme apart from the calibration interval is the root mean square error (RMSE) of the calibrated time series. The dependency of the RMSE on the calibration interval is shown in Fig. 10. The uncertainty of the isotope signals increases exponentially with increasing calibration interval for both instruments and both isotopes. For δ^{2}H the uncertainty increase is of similar extent for both instruments. The L1115-i accuracy of δ^{18}O is

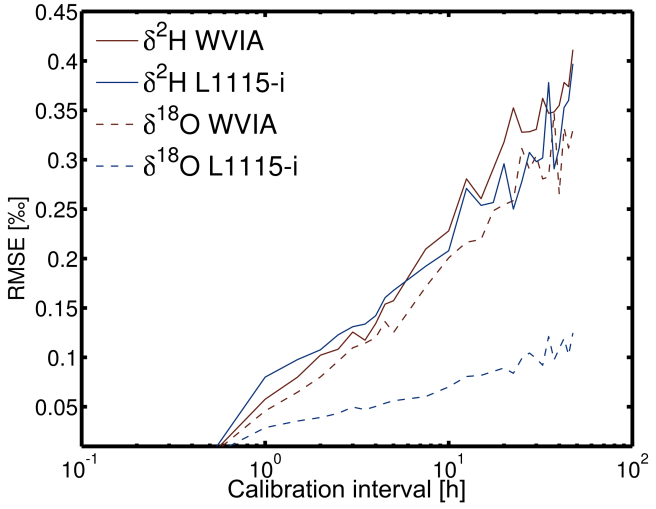

Fig. 10. Root mean square error (RMSE) of laser spectroscopic isotope measurements as a function of intercalibration time on a log scale.

however much better than the one of WVIA. Accurate and precise δ^{18}O measurements are essential for good quality-derived deuterium excess ($d = \delta^2\mathrm{H} - 8\delta^{18}\mathrm{O}$) signals. Thus, when choosing the optimum calibration interval, the δ^{18}O accuracy should be kept in mind.

6.3 Calibration strategy

Ideally, in order to avoid any effect of drift and to obtain the best possible accuracy of the measurements, the instruments should be calibrated at a frequency corresponding to the optimum calibration interval, for a duration corresponding to the optimum averaging time. However, a trade-off has to be made between minimum drift, maximum precision of the calibration runs and minimum measurement time consumption for calibration. Calibration with the standard delivery module built for the L1115-i system is time consuming due to the long equilibration phase in the vapouriser. With a two-point calibration run every 12 hours using two different standards at three different water vapour mixing ratios, one hour calibration time per day is needed in total. With such a calibration frequency at water vapour mixing ratios of around 15 700 ppmv, the precision of the L1115-i signal averaged to 15 min is $\sigma_A(\delta^2\mathrm{H}) = 0.06$ ‰ and $\sigma_A(\delta^{18}\mathrm{O}) = 0.01$ ‰ and the accuracy is 0.25 ‰ for δ^2H and 0.09 ‰ for δ^{18}O. With calibration runs performed every hour using the WVISS, the precision of the WVIA can be expected to be $\sigma_A(\delta^2\mathrm{H}) = 0.07$ ‰ and $\sigma_A(\delta^{18}\mathrm{O}) = 0.07$ ‰ and the accuracy becomes 0.08 ‰ for δ^2H and 0.07 ‰ for δ^{18}O. It has to be emphasised that these precision values were obtained in ideal laboratory conditions with well-controlled environmental parameters and thus represent an optimal case. They characterise the stability of the measurement system and do not account for the uncertainties introduced by water vapour mixing ratio biases discussed in Sect. 5.

7 Response Time of the measurement systems

The response time of a measurement system is an important characteristic of a laser spectroscopic instrument for field measurements of stable water isotopes. It serves as a design quantity for an optimal gas sampling system and determines the exact timing of the measurement. The primary aim of a good sampling system is to minimise interactions of the sample gas with the tubing material. The parameters influencing response time are the tubing material (Sturm and Knohl, 2010; Schmidt et al., 2010), temperature, tubing length as well as pumping rate.

The response time of the measurement system can be described using two temporal response components: a time lag, τ_{lag}, accounting for the retardation of the vapour sample in the tubing system and an exponential time constant, τ_{ads}, determined by the exchange rate of the gas in the optical cell, the effect of adsorption and desorption from the tubing surface as well as the very slow diffusion through the tubing walls. The time lag for the sample to reach the cavity can be derived from experimental data. It depends on the tubing length and the pumping rate of the individual instruments. In the setup used here, $\tau_{\mathrm{lag}} = 88$ s for the L1115-i instrument and 75 s for the WVIA system with a common 12 mm PFA sample line length of 15 m. The separation tubes leading to the individual instruments was 0.5 m long. Due to the difference in pumping rate of the two instruments, these short individual lines were not purged at the same rate. The flow in the common sampling line was 1 l min^{-1}. This explains the small difference in the lag times. In Fig. 11 the two time constants are schematically explained using an example of a response in δ^2H measured by L1115-i. The input signal to the measurement system can be described by a step-function, representing the switching of a valve between two reservoirs containing two gases with a different water vapour mixing ratio and isotopic composition. Here, step changes were done by switching between ambient laboratory water vapour and calibration vapour from the WVISS calibration unit.

The response function from the measurement system can be described approximately using the two time constants τ_{lag} and τ_{ads} and the concentration difference of the two samples (c_0, c_1). The concentration c_0 of the vapour before the switch is determined by averaging the data measured in the 30 s time period before the switch. The concentration after the switch is averaged from 4.5 min to 10 min (see Fig. 11, dashed lines). We use a simple model of gas exchange in a cavity assuming perfect mixing. The change in concentration, as measured by the instrument after a step change in the input signal from c_0 to c_1, can be described as follows:

$$c(t) = c_1 + (c_0 - c_1)\exp\left(-\frac{t - \tau_{\mathrm{lag}}}{\tau_{\mathrm{ads}}}\right). \quad (7)$$

Table 6. Key characteristics of the short-term stability of laser spectroscopic isotope measurements. σ_A is the Allan deviation. τ_0 is the optimal integration time.

Instrument	L1115-i		L2130-i		WVIA		WVIA-EP	
	δ^2H	δ^{18}O	δ^2H	δ^{18}O	δ^2H	δ^{18}O	δ^2H	δ^{18}O
τ_0 [min]	15	50	170	100	10	170	7	30
$\sigma_A^{\tau_0}$ [‰]	0.06	0.01	0.02	0.006	0.07	0.07	0.02	0.01
σ_A^{5s} [‰]	0.57	0.17	0.83	0.22	0.43	0.19	0.53	0.19

Table 7. Average response times in s and corresponding standard deviations for the L1115-i and the WVIA instrument and the different water isotopic species. In total 103 switching experiments were performed: 54 switches to higher water concentrations (switch up, τ_{up}) and 49 switches to lower concentrations (switch down, τ_{down}).

	Picarro		WVIA	
	τ_{up} [s]	τ_{down} [s]	τ_{up} [s]	τ_{down} [s]
δ^2H	29 ± 3	43 ± 4	3.3 ± 0.3	5.7 ± 2.5
δ^{18}O	20 ± 3	30 ± 3	2.0 ± 0.3	4.1 ± 2.5
H_2O	15 ± 2	16 ± 3	2.5 ± 0.2	3.3 ± 2.1

This theoretical response function is fitted by least squares with quality criteria of a root mean square error of $RMSE_{\delta^{18}O}$ <2 ‰, $RMSE_{\delta^2H}$ <10 ‰, and $RMSE_{H_2O}$ <1000 ppmv. For the fitting, the data obtained during the first two minutes of the response are weighted by a factor of 10, thus ensuring that slight oscillations in the equilibrium value c_0 do not affect the estimated response time τ_{ads} substantially. The fitting procedure serves as a quality control of the switches and allows to eliminate step changes, during which the calibration unit did not work properly, due to blocking of the capillary tubing or air pump problems. The exponential time constant τ_{ads} of the response signals is calculated separately for the water vapour mixing ratio, δ^{18}O and δ^2H. Step changes of $\sim$ 60 ‰ in δ^2H (between −80 ‰ and −140 ‰), ∼7 ‰ in δ^{18}O (between −25 ‰ and −32‰) and ∼1000 ppmv in H_2O (between 12 000 ppmv and 22 000 ppmv) were performed for external tubing temperatures of 30 °C (18 steps), 60 °C (48 steps), 90°C (38 steps) and 120 °C (8 steps). The temperature of the heated tubing (Lohmann Wärmetechnik und Regelung, Graz) was regulated at the splitting end between L1115-i and WVIA using a R1140 regulator (Elotech, Germany) with a SIRIUS SC semiconductor contactor (Siemens, Germany).

The response times τ_{ads} for δ^2H , δ^{18}O and H_2O averaged over all performed step changes in water vapour signal differ and amount to 36 s, 25 s, and 15 s for L1115-i and 4.5 s, 3 s and 2.9 s for WVIA, respectively. Schmidt et al. (2010) found that the response time of δ^2H lags behind the one of δ^{18}O by a factor of 1.7–3.3 using a PFA tubing, which is more than the factor of 1.5 ± 0.1 found here for both L1115-i and WVIA also using PFA tubing. The difference in the response times of the isotopes has implications for the computation of deuterium excess. During a step change in water vapour mixing ratio and isotope concentration, the signals of water vapour mixing ratio and the two heavy isotopes reach the new target values, when the equilibrium between the pipe gas and the adsorbed phase on the tubing wall has been re-established. The longer response times for the heavy isotopes compared to the bulk water concentration are evidence for longer interaction time scales of the heavy isotopes with the tubing and cavity walls and thus a higher affinity with the material.

In this experiment the external tubing effects were the same for both instruments. Internal memory effects induced by adsorption on tubing and the cavity wall of the

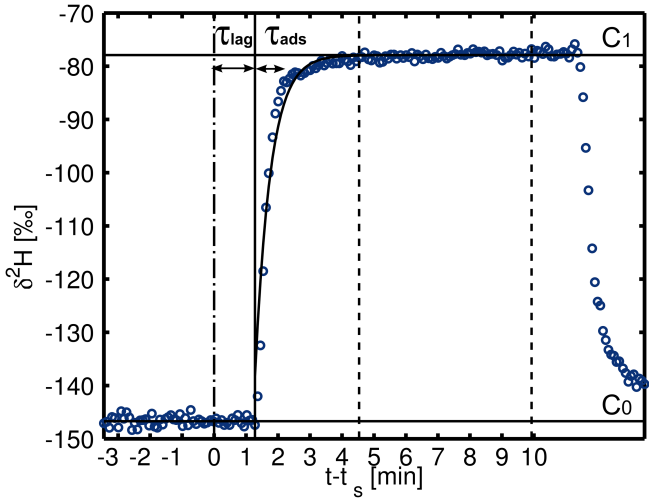

Fig. 11. Example of a response to a step change in δ^2H as measured by the L1115-i instrument. The total system response time consists of a time lag τ_{lag}, which depends on the tubing length and pumping rate and an exponential time constant τ_{ads} characterising the measured change in concentration from C_0 to C_1, determined by the cavity gas exchange rate and the adsorption-desorption equilibrium on the tubing and cavity walls. The dashed lines delimit the data used for computing the concentration after the switch C_1. The black dashed dotted line indicates the switch time of the valve, the black full line indicates the instant when the vapour front of the new sample arrives in the cavity.

instruments were however different. The 5–10 times smaller response times of WVIA compared to L1115-i indicate that the influence of the external tubing on the memory effect of the measurement systems is small. The typical residence time of the gas in the measurement cell is shorter for the WVIA instrument than for L1115-i. Additionally, the lower surface-to-volume ratio of the WVIA cavity compared to the L1115-i cavity implies that surface effects are less important in the WVIA. Thus, the internal tubing and especially the cavity exchange rate are the central elements determining response time, if hydrophobic material like PFA is used for the external tubing.

In our experimental setup, a step towards lower water vapour mixing ratios always corresponds to a step towards more depleted isotope values, which implies that both water and isotope fluxes between the wall and the bulk gas in the tubing have the same direction. During a step change from high to low water and isotope concentration (switch down), water molecules desorb from the tubing and cavity walls. A step change towards higher water and isotope concentration implies adsorption of water molecules on the tubing and cavity material.

In Table 7 the average response times for L1115-i and WVIA are shown separately for switch up (τ_{up}) and switch down (τ_{down}) experiments. The response times for the heavy isotope signals are ∼50 % larger in the case of desorption (switch down) than for adsorption (switch up). The desorption process is thus more strongly retarding heavy isotopic molecules than adsorption. The difference in response times between switch up and switch down steps is however much smaller for the water vapour mixing ratio signal. The absolute difference in isotopic composition between the vapour sources (step size) was varied using different standards, but no correlation between the step size and the response times was found (not shown).

The adsorption and desorption processes are temperature-dependent (Oura et al., 2003), and thus higher tubing wall temperatures may reduce response times. The panels of Fig. 12 show the distribution of the obtained response times for L1115-i computed from the performed step changes as a function of external tubing temperature for δ^2H, δ^{18}O and H_2O. For example, in the case of δ^2H in Fig. 12a, the obtained average response time decreases with increasing temperature. In Fig. 12 the response times for the different isotope signals are separately shown for switch down cases (left panels) and switch up cases (right panels). We find that temperature only slightly influences the time scale of the desorption process with a decreasing tendency of the response time of δ^2H with increasing temperatures (Fig. 12a). The response time of the δ^2H signal is 11 % smaller on average with a tubing temperature of 120°C than with a tubing temperature of 30 °C. This temperature effect is weaker for δ^{18}O with a 6 % decrease in response time between a tubing temperature of 30 °C and 120 °C (Fig. 12c). The temperature effect observed for the switch down cases is not as strong in the switch up

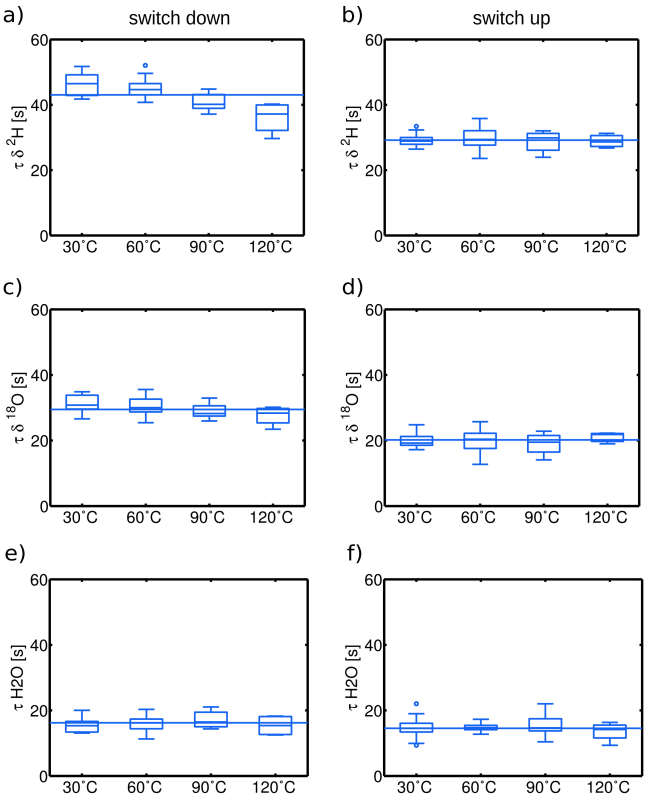

Fig. 12. Typical response times τ_{ads} for the L1115-i isotope measurements. The boxplots show the distribution of response times as a function of tubing temperature. The left column of plots shows switches to lower water vapour mixing ratios (switch down) and the right column of plots shows switches to higher water vapour mixing ratios (switch up).

cases. In general, temperature effects observed in Fig. 12 are small in the range of 30 °C to 120 °C. Thus, the sampling line heating is needed primarily to avoid condensation and does not reduce response times significantly.

For both laser systems used here, we found that it is not the acquisition time that determines the highest possible temporal resolution of the measurements, but the exchange rate of the cavity and the interaction timescale of the water molecules with the tubing and cavity walls. Thus, the choice of the tubing material and the flow rate through the sampling system are central aspects of an isotope measurement setup. A good knowledge of the response time distribution of each isotope signal allows to correct for biases introduced by the sampling system and provides a framework for the uncertainty assessment of high frequency variations in δ^{18}O, δ^2H and deuterium excess.

No significant improvements or changes were found in the L2130-i and WVIA-EP with respect to response times.

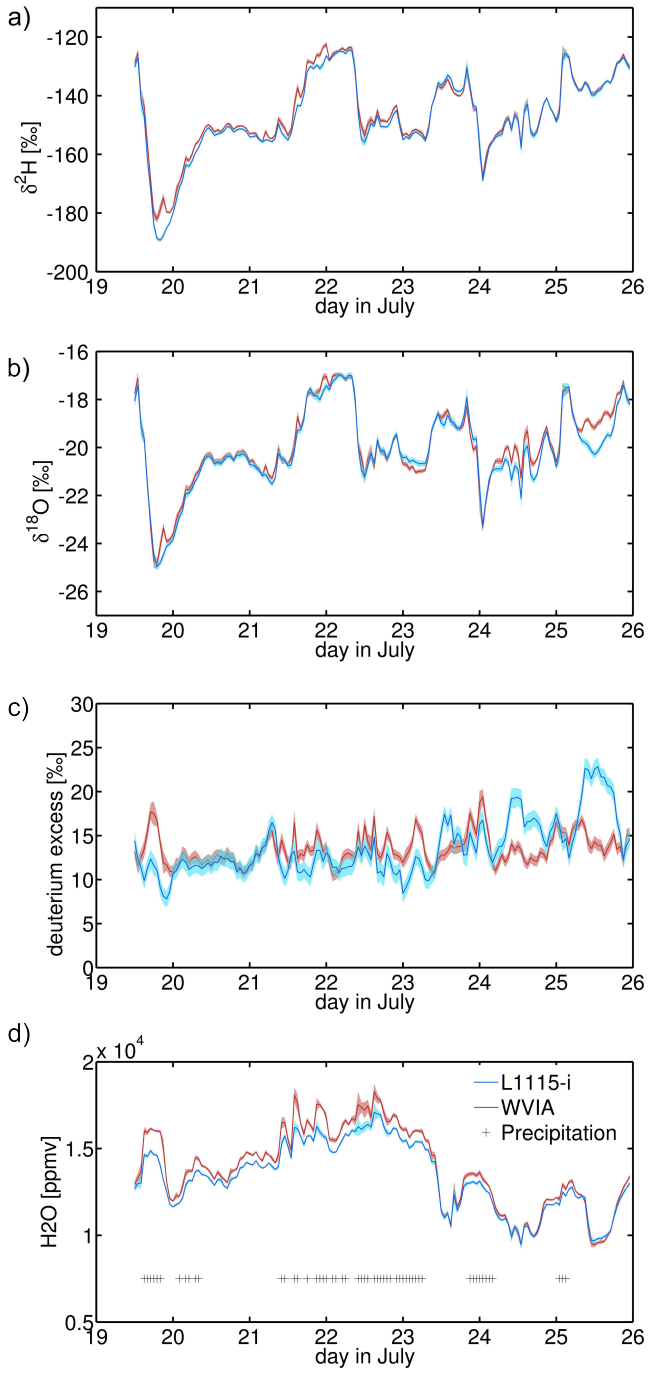

Fig. 13. Time series of δ^2H **(a)**, δ^{18}O **(b)**, deuterium excess **(c)** and water vapour mixing ratio **(d)** from ambient air measurements in Zurich from 19–26 July 2011 with L1115-i in blue and WVIA in red. The data were averaged to 1 h and the shaded area shows the 1 h standard deviation based on 5 s measured data for L1115-i and 5 s averaged data for WVIA. Crosses in **(d)** indicate the occurrence of precipitation.

8 Comparative ambient air measurements

As a verification of the laboratory characterisation experiments, comparative ambient air measurements were done on the roof of a tower building in Zurich (47.38°, 8.55°, ∼500 m a.s.l.) in the period 19–26 July 2011 with both L1115-i and WVIA connected to the same inlet. The L1115-i was set up in a dedicated box outside with a short stainless steel sampling line of 70 cm length with an outer diameter of 1/8 inch. The WVIA was set up in a room, and a 23-m-long PTFE sampling line with an outer diameter of 1/4 inch was used.

The L1115-i was calibrated using the SDM by performing two calibrations per day at 3 pm and 3 am for ∼1 h in total using WS 6 and WS 7 (Table 2). Calibrations were performed at the ambient water vapour mixing ratio conditions as well as 3000 ppmv above and 3000 ppmv below ambient water vapour mixing ratios. If variations in water vapour mixing ratio during the day were >1000 ppmv, the corrections found in Sect. 5 (i.e. Eqs. 4 and 5) were applied. The average standard deviation of the calibration runs was 0.8 ‰ for δ^2H and 0.2 ‰ for δ^{18}O. These values compare well with the uncertainty estimates obtained in Sect. 3 in the delta-scale laboratory experiment. The optimum precision values described by the Allan deviation should however not be compared directly to these sample standard deviations.

For the WVIA, calibration runs were performed every 15 min for 2 min using WS 6 (Table 2). The water vapour mixing ratio correction function was determined once on 19 July and once on 26 July using the WVISS by measuring WS 6 at different water vapour mixing ratios in the range 5000–25 000 ppmv. The average standard deviation of the calibration runs was 1.3 ‰ for δ^2H and 0.6 ‰ for δ^{18}O.

During the measurement period weather conditions were very variable with a cold front passage in the evening of 19 July 2011 and with intermittent rainfall for the whole period (black crosses in Fig. 13d). The sky was almost constantly overcast with a cloud base of about 1500 m. Some longer periods of intermittent sunshine occurred especially on the 24 and 25 July 2011. Air temperature varied between 12 °C during nighttime and around 22 °C at midday.

The measured isotopic composition of vapour varied in the range −180 ‰ to −125 ‰ for δ^2H and −26 ‰ to −18 ‰ for δ^{18}O (Figs. 13a,b). The data were averaged to 1 h and the shaded area shows the 1 h standard deviation based on 5 s measured data for L1115-i and 5 s averaged data for WVIA. The correspondence of the isotopic measurements of the two instruments was good with root mean square differences of 2.3 ‰ for δ^2H and 0.5 ‰ for δ^{18}O. On some days larger differences can be observed, e.g. on 24 and especially 25 July around midday in δ^{18}O. This mismatch of ∼1 ‰ in δ^{18}O leads to a difference of nearly 10 ‰ in deuterium excess (Fig. 13c), which is otherwise in good agreement between the two instruments with an RMSE of 3.1 ‰. The strong deviations on the 24 July and 25 July are responsible

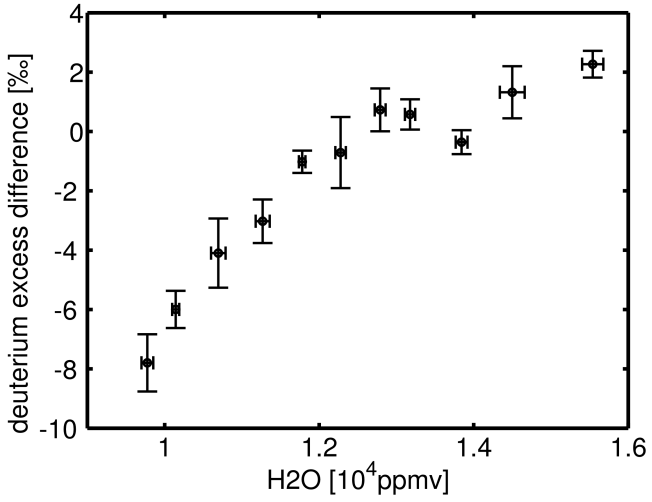

Fig. 14. Dependency of the deuterium excess difference between L1115-i and WVIA on the ambient water vapour mixing ratio during the comparative field measurement on the roof of a tower building in Zurich from 19–26 July 2011.

for the low correlation between the deuterium excess measurements of the two instruments ($\rho(d) = 0.38$) and are due to low water vapour mixing ratios. The range of measured water vapour mixing ratios was 1000 ppmv to 16 000 ppmv (Fig. 13d). The discrepancy between L1115-i and WVIA is clearly water vapour mixing ratio- dependent (Fig. 14). At lower water vapour mixing ratios, the difference between the two signals is larger, which highlights the crucial importance of good water vapour mixing ratio dependency corrections. For L1115-i these corrections were done continuously; for WVIA the water vapour mixing ratio dependency was tested once on the 19 July and once on the 26 July, and no significant change between these two measurements could be observed. Another effect, which is linked to the water vapour mixing ratio, is the interference of hydrocarbons and especially methane (Galewsky et al., 2011). The lower the water vapour mixing ratio, the stronger the interference of such trace gases. In the spectral region used in both L1115-i and WVIA, the interference with methane is strong (Rothman et al., 2009) and it may be slightly different for the two instruments, which could explain the 1 ‰ deviation in δ^{18}O. This methane cross-talk effect is taken into account in the spectral fitting of the new Picarro version L2130-i. No methane measurements were done during this campaign. The cross-talk effect between water isotope measurements in water vapour and methane, if relevant, could not be corrected for.

9 Conclusions

This paper presents a characterisation study of laser spectroscopic measurements of stable isotopes in ambient water vapour. We used two commercial versions of two laser spectroscopic systems as well as comparative IRMS measurements. The laser spectroscopic instruments used were two systems by Picarro (versions L1115-i and L2130-i) and two systems by Los Gatos Research (WVIA, WVIA-EP). The main properties of the laser measurement systems investigated here were biases due to water concentration effects, the short and long-term precision and accuracy, and response times.

The assessments presented in this paper were all pursued with the final aim of obtaining a comprehensive picture of the uncertainty of high frequency water vapour isotope measurements using field-deployable laser spectroscopic instruments. We found that a large part of the measurement uncertainty depends on how the instruments are calibrated, more specifically on the calibration technique and strategy.

The inherent precision of the Picarro L1115-i instrument is dependent on water vapour mixing ratio. In general, we found higher measurement uncertainties for lower water vapour mixing ratios. This represents the basic uncertainty of the measurement. Other uncertainty sources are then superimposed and depend on the sampling procedure and calibration. The uncertainty of the calibration vapour production system adds to the basic measurement uncertainty. An overall estimate of the bottom-up uncertainty is difficult to obtain as the different error components cannot be estimated independently. The assessments of the different uncertainty components however allow us to determine an optimal calibration procedure for the instruments of the two manufacturers Picarro and Los Gatos, which is a trade-off between maximum ambient air measurement time, maximum precision of the calibration run, typically requiring long calibration runs (10–30 min) and a minimum calibration interval to regularly update calibration factors.

The precision at optimum averaging time is $\sigma_A^{\tau_0=15\,\mathrm{min}}(\delta^2\mathrm{H}) = 0.06\,‰$ and $\sigma_A^{\tau_0=50\,\mathrm{min}}(\delta^{18}\mathrm{O}) = 0.01\,‰$ for L1115-i and $\sigma_A^{\tau_0=10\,\mathrm{min}}(\delta^2\mathrm{H}) = 0.07\,‰$ and $\sigma_A^{\tau_0=7\,\mathrm{min}}(\delta^{18}\mathrm{O}) = 0.07\,‰$ for WVIA at 15 700 ppmv water vapour mixing ratio. The measurement precision of both instruments is better in the new versions L2130-i and WVIA-EP. In both new instrument versions, Allan deviations at optimum averaging time are smaller compared to the ones found for the previous versions.

We performed two top-down assessments of uncertainty by comparing the calibration measurements of 10 standards as well as ambient air measurement by the WVIA and L1115-i instruments. From the field measurements we obtained root mean square deviations between the two instruments of $\mathrm{RMSE}(\delta^2\mathrm{H}) = 2.3\,‰$ and $\mathrm{RMSE}(\delta^{18}\mathrm{O}) = 0.5\,‰$. The delta-scale linearity experiment showed that repeated measurements of 10 standards lead to uncertainties of on average 1.7 ‰ (1.0 ‰) for δ^2H and 0.5 ‰ (0.4 ‰) for δ^{18}O for L1115-i (WVIA). IRMS is typically characterised by similar or slightly smaller uncertainties than found here for the L1115-i and WVIA systems.

The uncertainty of deuterium excess resulting from ambient measurements done with the well-characterised laser spectrometers used here was 3.1 ‰. This uncertainty will probably be reduced in upcoming versions of commercial instruments, owing to improved spectral fitting algorithms with respect to water vapour mixing ratio dependencies and interfering trace gases.

In summary, from the experiments presented in this paper we can formulate the following recommendations for the use of laser spectrometric systems to measure ambient water vapour isotopes during field campaigns:

1. Calibration runs should be done regularly and ideally at the same water vapour mixing ratio as the measurements. For the L1115-i we perform a two-point calibration run every 12 h using 2 different standards at 3 different water vapour mixing ratios, which takes 1 h calibration time per day in total. For the WVIA, calibration runs should be performed hourly for 5–10 min to obtain the highest possible accuracy.

2. Water vapour mixing ratio effects should be quantified for old versions of the laser spectrometers. These effects are different for each instrument, and the correction functions found in this study have no general validity. In the new version of the Picarro instrument (L2130-i), however, the water vapour mixing ratio dependency of isotope measurements is very small and corrections are not necessary except if measurements are performed in very dry conditions.

3. Dried ambient air is recommended as a carrier gas for calibration, because its trace gas composition is equivalent to the measured gas sample. Residual ambient water can be a problem when calibrating at very low water vapour mixing ratios. In this case laboratory tests with other carrier gases can be helpful.

4. If high frequency measurements are used, response time differences in $\delta^{18}O$ and $\delta^{2}H$ should be accounted for. These depend on the setup and the tubing material used and have to be quantified experimentally. We found that response times were 1.5 times larger for $\delta^{2}H$ than for $\delta^{18}O$ and 10 times larger for L1115-i than for WVIA. The response times of the measured signals depend on the exchange rate of the measurement cell and tubing systems as well as the material affinity of the isotopes. However, no clear dependency of the response times on tubing temperature was found.

5. To obtain high accuracy water vapour mixing ratio measurements with uncertainties smaller than 500 ppmv, regular calibration of the water vapour mixing ratio measurements is suggested.

Acknowledgements. We are grateful to the anonymous referees for their detailed and constructive remarks. We thank Roland Werner from the Institute of Agricultural Sciences, ETH for the IRMS measurements of our standards, Aaron van Pelt and Gregor Hsiao from Picarro and Doug Baer from LGR for technical support as well as Edwin Hausammann and Uwe Weers for technical help in the lab. Patrick Sturm and Alexander Knohl were funded by a Marie Curie Excellence Grant of the European Commission (Project No: MEXT-CT-2006-042268).

Edited by: P. Werle

References

Allan, D. W.: Statistics of atomic frequency standards, Proc. IEEE, 54, 221–230, doi:10.1109/PROC.1966.4634, 1966.

Araguas, L. A., Danesi, P., Froehlich, K., and Rozanski, K.: Global monitoring of the isotopic composition of precipitation, J. Radioanal. Nucl. Ch., 205, 189–200, 1996.

Baer, D. S., Paul, J. B., Gupta, M., and O'Keefe, A.: Sensitive absorption measurements in the near-infrared region using off-axis integrated-cavity output spectroscopy, Appl. Phys. B-Lasers O., 75, 261–265, 2002.

Brand, W. A., Geilmann, H., Crosson, E. R., and Rella, C. W.: Cavity ring-down spectroscopy versus high-temperature conversion isotope ratio mass spectrometry; a case study on $\delta^{2}H$ and $\delta^{18}O$ of pure water samples and alcohol/water mixtures, Rapid Commun. Mass. Sp., 23, 1879–1884, doi:10.1002/rcm.4083, 2009.

Ciais, P. and Jouzel, J.: Deuterium and oxygen 18 in precipitation: isotopic model, including mixed cloud processes, J. Geophys. Res.-Atmos., 99, 16793–16803, 1994.

Craig, H.: Isotopic variations in meteoric waters, Sci. J., 133, 1702–1703, 1961.

Crosson, E. R.: A cavity ring-down analyzer for measuring atmospheric levels of methane, carbon dioxide and water vapor, Appl. Phys. B-Lasers O., 92, 403–408, 2008.

Dansgaard, W.: Stable isotopes in precipitation, Tellus, 16, 436–468, 1964.

Dansgaard, W., Johnsen, S. J., Clausen, H. B., Dahl-Jensen, D., Gundestrup, N. S., Hammer, C. U., Hvidberg, C. S., Steffensen, J. P., Sveinbjörnsdottir, A. E., Jouzel, J., and Bond, G.: Evidence for general instability in past climate from a 250-kyr ice-core record, Nature, 364, 218–220, 1993.

Dongmann, G., Nürnberg, H. W., Förstel, H., and Wagener, K.: On the enrichment of $H_2{}^{18}O$ in the leaves of transpiring plants, Radiat. Environ. Bioph., 11, 41–52, 1974.

Dyroff, C., Fütterer, D., and Zahn, A.: Compact diode-laser spectrometer ISOWAT for highly sensitive airborne measurements of water-isotope ratios, Appl. Phys. B, 98, 537-548, 2010.

Farquhar, G. D., Cernusak, L. A., and Barnes, B.: Heavy water fractionation during transpiration, Plant Physiol., 143, 11–18, 2007.

Federer, B., Brichet, N., and Jouzel, J.: Stable isotopes in hailstones. 1. The isotopic cloud model, J. Atmos. Sci., 39, 1323–1335, 1982.

Field, R. D., Jones, D. B. A., and Brown, D. P.: Effects of postcondensation exchange on the isotopic composition of water in the atmosphere, J. Geophys. Res.-Atmos., 115, D24305, doi:10.1029/2010JD014334, 2010.

Galewsky, J., Rella, C., Sharp, Z., Samuels, K., and Ward, D.: Surface measurements of upper tropospheric water vapor isotopic composition on the Chajnantor Plateau, Chile, Geophys. Res. Lett., 38, L17803, doi:10.1029/2011GL048557, 2011.

Gat, J. R.: Oxygen and hydrogen isotopes in the hydrological cycle, Annu. Rev. Earth Pl. Sc., 24, 225–262, 1996.

Gat, J. R. and Dansgaard, W.: Stable isotope survey of the freshwater occurrences in Israel and the Jordan Rift Valley, J. Hydrol., 16, 177–211, 1972.

Gat, J. R., Klein, B., Kushnir, Y., Roether, W., Wernli, H., Yam, R., and Shemesh, A.: Isotope composition of air moisture over the Mediterranean Sea: an index of the air-sea interaction pattern, Tellus B, 55, 953–965, 2003.

Gehre, M., Geilmann, H., Richter, J., Werner, R., and Brand, W.: Continuous flow $^2H/^1H$ and $^{18}O/^{16}O$ analysis of water samples with dual inlet precision, Rapid Commun. Mass Sp., 18, 2650–2660, doi:10.1002/rcm.1672, 2004.

Gianfrani, L., Gagliardi, G., van Burgel, M., and Kerstel, E. R. T.: Isotope analysis of water by means of near-infrared dual-wavelength diode laser spectroscopy, Opt. Express, 11, 1566–1576, 2003.

Gonfiantini, R.: Standards for stable isotope measurements in natural compounds, Nature, 271, 534–536, 1978.

Gupta, P., Noone, D., Galewsky, J., Sweeney, C., and Vaughn, B. H.: Demonstration of high-precision continuous measurements of water vapor isotopologues in laboratory and remote field deployments using wavelength-scanned cavity ring-down spectroscopy (WS-CRDS) technology, Rapid Commun. Mass. Sp., 23, 2534–2542, 2009.

Han, L.-F., Groening, M., Aggarwal, P., and Helliker, B. R.: Reliable determination of oxygen and hydrogen isotope ratios in atmospheric water vapour adsorbed on 3A molecular sieve, Rapid Commun. Mass. Sp., 20, 3612–3618, doi:10.1002/rcm.2772, 2006.

He, H. and Smith, R. B.: An advective-diffusive isotopic evaporation-condensation model, J. Geophys. Res.-Atmos., 104, 18619–18630, 1999.

Helliker, B. R. and Noone, D.: Novel approaches for monitoring of water vapor isotope ratios: plants, lasers and satellites, in: Isoscapes: Understanding Movement, Pattern, and Process on Earth Through Isotope Mapping, edited by: West, J. B., Chap. 4, 71–87, Springer Science, 2010.

Hendry, M. J., Richman, B., and Wassenaar, L. I.: Correcting for methane interferences on δ^2H and $\delta^{18}O$ measurements in pore water using H_2O liquid-H_2O vapor equilibration laser spectroscopy., Anal Chem., 83, 5789–5796, 2011.

Horita, J. and Kendall, C.: Stable isotope analysis of water and aqueous solutions by conventional dual-inlet mass spectrometry, in: Handbook of Stable Isotope Analytical Techniques, edited by: de Groot, P. A., Vol. 1, Chap. 1, 1–37, Elsevier, 2004.

IAEA: Reference Sheet for VSMOW2 and SLAP2 international measurement standards, International Atomic Energy Agency (IAEA), 2009.

Iannone, R. Q., Romanini, D., Kassi, S., Meijer, H. A. J., and Kerstel, E. R. T.: A microdrop generator for the calibration of a water vapor isotope ratio spectrometer, J. Atmos. Ocean Tech., 26, 1275–1288, doi:10.1175/2008JTECHA1218.1, 2009.

Johnsen, S. J., Dahl-Jensen, D., Gundestrup, N., Steffensen, J. P., Clausen, H. B., Miller, H., Masson-Delmotte, V., Sveinbjörnsdottir, A. E., and White, J.: Oxygen isotope and palaeotemperature records from six Greenland ice-core stations: Camp Century, Dye-3, GRIP, GISP2, Renland and NorthGRIP, J. Quaternary Sci., 16, 299–307, 2001.

Johnson, L. R., Sharp, Z. D., Galewsky, J., Strong, M., Van Pelt, A. D., Dong, F., and Noone, D.: Hydrogen isotope correction for laser instrument measurement bias at low water vapor concentration using conventional isotope analyses: application to measurements from Mauna Loa Observatory, Hawaii, Rapid Commun. Mass. Sp., 25, 608–616, doi:10.1002/rcm.4894, 2011.

Jouzel, J., Alley, R. B., Cuffey, K. M., Dansgaard, W., Grootes, P., Hoffmann, G., Johnsen, S. J., Koster, R. D., Peel, D., Shuman, C. A., Stievenard, M., Stuiver, M., and White, J.: Validity of the temperature reconstruction from water isotopes in ice cores, J. Geophys. Res.-Oceans, 102, 26471–26487, 1997.

Kerstel, E. R. T.: Isotope Ratio Infrared Spectrometry, in: Handbook of Stable Isotope Analytical Techniques, edited by: De Groot, P. A., chap. 34, 759–787, Elsevier, 2004.

Kerstel, E. R. T. and Gianfrani, L.: Advances in laser-based isotope ratio measurements: selected applications, Appl. Phys. B-Lasers O., 92, 439–449, 2008.

Kerstel, E. R. T., Gagliardi, G., Gianfrani, L., Meijer, H. A. J., van Trigt, R., and Ramaker, R.: Determination of the $^2H/^1H$, $^{17}O/^{16}O$, and $^{18}O/^{16}O$ isotope ratios in water by means of tunable diode laser spectroscopy at 1.39 µm, Spectrochim. Acta A, 58, 2389–2396, 2002.

Kerstel, E. R. T., Iannone, R. Q., Chenevier, M., Kassi, S., Jost, H. J., and Romanini, D.: A water isotope (^2H, ^{17}O, and ^{18}O) spectrometer based on optical feedback cavity-enhanced absorption for in situ airborne applications, Appl. Phys. B-Lasers O., 85, 397–406, doi:10.1007/s00340-006-2356-1, 2006.

Lee, J.-E. and Fung, I.: "Amount effect" of water isotopes and quantitative analysis of post-condensation processes, Hydrol. Process., 22, 1–8, doi:10.1002/hyp.6637, 2008.

Lee, X., Sargent, S., Smith, R., and Tanner, B.: In situ measurement of the water vapor $^{18}O/^{16}O$ isotope ratio for atmospheric and ecological applications, J. Atmos. Ocean Tech., 22, 555–565, 2005.

Lis, G., Wassenaar, L. I., and Hendry, M. J.: High-precision laser spectroscopy D/H and $^{18}O/^{16}O$ measurements of microliter natural water samples, Anal. Chem., 80, 287–293, 2008.

Oura, K., Lifshits, V. G., Saranin, A. A., Zotov, A. V., and Katayama, M.: Surface Science: An Introduction, Springer, Berlin, 2003.

Paldus, B. A. and Kachanov, A. A.: An historical overview of cavity-enhanced methods, Can. J. Phys., 83, 975–999, 2005.

Paul, J. B., Lapson, L. and Anderson, J. G.: Ultrasensitive Absorption Spectroscopy with a High-Finesse Optical Cavity and Off-Axis Alignment, Appl. Opt., 40, 4904–4910, 2001.

Pfahl, S. and Wernli, H.: Air parcel trajectory analysis of stable isotopes in water vapor in the eastern Mediterranean, J. Geophys. Res.-Atmos., 113, D20104, doi:10.1029/2008JD009839, 2008.

Rambo, J., Lai, C.-T., Farlin, J., Schroeder, M., and Bible, K.: On-site calibration for high precision measurements of water vapor isotope ratios using off-axis cavity-enhanced absorption spectroscopy, J. Atmos. Ocean Tech., 28, 1448–1457, doi:10.1175/JTECH-D-11-00053.1, 2011.

Rothman, L. S., Gordon I. E., Barbe, A., Chris Benner, D., Bernath, P. F., Birk, M., Boudon, V., Brown, L. R., Cam-

pargue, A., Champion, J.-P., Chance, K., Coudert, L. H., Dana, V., Devi, V. M., Fally, S., Flaud, J.-M., Gamache, R. R., Goldmanm, A., Jacquemart, D., Kleiner, I., Lacome, N., Lafferty, W. J., Mandin, J.-Y., Massie, S. T., Mikhailenko, S. N., Miller, C. E., Moazzen-Ahmadi, N., Naumenko, O. V., Nikitin, A. V., Orphal, J., Perevalov, V. I., Perrin, A., Predoi-Cross, A., Rinsland, C. P., Rotger, M., Šimečková, M., Smith, M. A. H., Sung, K., Tashkun, S. A., Tennyson, J., Toth, R. A., Vandaele, A. C., and Vander Auwera, J.: The HITRAN 2008 molecular spectroscopic database, J. Quant. Spectrosc. Ra., 110, 533–572, 2009.

Sayres, D. S., Moyer, E. J., Hanisco, T. F., St Clair, J. M., Keutsch, F. N., O'Brien, A., Allen, N. T., Lapson, L., Demusz, J. N., Rivero, M., Martin, T., Greenberg, M., Tuozzolo, C., Engel, G. S., Kroll, J. H., Paul, J. B., and Anderson, J. G.: A new cavity based absorption instrument for detection of water isotopologues in the upper troposphere and lower stratosphere, Rev. Sci. Instrum., 80, 044102, doi:10.1063/1.3117349, 2009.

Schmidt, M., Maseyk, K., Lett, C., Biron, P., Richard, P., Bariac, T., and Seibt, U.: Concentration effects on laser-based δ^{18}O and δ^{2}H measurements and implications for the calibration of vapour measurements with liquid standards, Rapid Commun. Mass. Sp., 24, 3553–3561, doi:10.1002/rcm.4813, 2010.

Sodemann, H., Masson-Delmotte, V., Schwierz, C., Vinther, B. M., and Wernli, H.: Interannual variability of Greenland winter precipitation sources: 2. Effects of North Atlantic Oscillation variability on stable isotopes in precipitation, J. Geophys. Res.-Atmos., 113, D12111, doi:10.1029/2007JD009416, 2008.

Strong, M. Z. D., Sharp, D., and Gutzler, D. S.: Diagnosing moisture transport using D/H ratios of water vapor, Geophys. Res. Lett., 34, L03404, doi:10.1029/2006GL028307, 2007.

Sturm, P. and Knohl, A.: Water vapor δ^{2}H and δ^{18}O measurements using off-axis integrated cavity output spectroscopy, Atmos. Meas. Tech., 3, 67–77, doi:10.5194/amt-3-67-2010, 2010.

Uemura, R., Matsui, Y., Yoshimura, K., Motoyama, H., and Yoshida, N.: Evidence of deuterium excess in water vapor as an indicator of ocean surface conditions, J. Geophys. Res.-Atmos., 113, D19114, doi:10.1029/2008JD010209, 2008.

Wang, L., Caylor, K. K., and Dragoni, D.: On the calibration of continuous, high-precision δ^{18}O and δ^{2}H measurements using an off-axis integrated cavity output spectrometer, Rapid Commun. Mass Sp., 23, 530–536, doi:10.1002/rcm.3905, 2009.

Webster, C. R. and Heymsfield, A. J.: Water Isotope Ratios D/H, ^{18}O/^{16}O, ^{17}O/^{16}O in and out of Clouds Map Dehydration Pathways , Science, 302, 1742, doi:10.1126/science.1089496, 2003.

Wen, X. F., Sun, X. M., Zhang, S. C., Yu, G. R., Sargent, S. D., and Lee, X.: Continuous measurement of water vapor D/H and ^{18}O/^{16}O isotope ratios in the atmosphere, J. Hydrol., 349, 489–500, 2008.

Werle, P.: Accuracy and precision of laser spectrometers for trace gas sensing in the presence of optical fringes and atmospheric turbulence., Appl. Phys. B-Lasers O., 102, 313–329, 2011.

Yakir, D. and Wang, X.-F.: Fluxes of CO_2 and water between terrestrial vegetation and the atmosphere estimated from isotope measurements, Nature, 380, 515–517, 1996.

Yepez, E. A., Williams, D. G., Scott, R. L., and Lin, G.: Partitioning overstory and understory evapotranspiration in a semiarid savanna woodland from the isotopic composition of water vapor, Agr. Forest Meteorol., 119, 53–68, 2003.